ULTRASONIC SIMULATION OF MSBLS MULTIPATH FADING FOR ORBITER LANDING CONFIGURATION

(FINAL REPORT)

by

Dr. H. S. Hayre

Work Done Under

NASA Contract NAS 9 - 11845

February 28, 1978

TECHNICAL MONITOR

Howard C. Kyle
MSBLS - GS Project Manager
NASA - L.B.J. Space Center
Houston, Texas 77058

UNIVERSITY OF HOUSTON

WAVE PROPAGATION LAB. - ELECTRICAL ENGINEERING DEPT.

CULLEN COLLEGE OF ENGINEERING DEPT.

HOUSTON, TEXAS 77004

TEL: AC 713-749-4503/4535/4534

LISTS OF CONTENTS

LIST OF FIGURES

LIST OF TABLES

2. ACKNOWLEDGMENTS

The Wave Propagation Laboratory - Electrical Engineering Department, University of Houston is indeed thankful to the NASA - Lyndon B. Johnson Space Center, Houston, Texas, for support of this work, and Howard C. Kyle and late James Satterfield for project coordination and monitoring for NASA. Technical input and support by other NASA personnel and its contractor Lockheed Electronics Company in all phases of this work are sincerely appreciated. Significant results of this ultrasonic simulation effort are relevant to many other landing/guidance and control signal systems used by other government agencies. A use of these results and, of course the technique of ultrasonic simulation itself are expected to enhance the operational capabilities of such systems and help update their design.

3. SUMMARY

An Ultrasonic Simulation of Orbiter, and it's Microwave Scanning Beam Landing System (MSBLS), the runway and rain environment were performed in order to determine the multipath fading from the ground, and its possible degrading effect on the orbiter received beam shape and the associated landing guidance parameters.

The on-shuttle antenna pattern of the MSBLS receiver, $-40° \leq \phi \leq +40°$, $-23° \leq \theta \leq +27°$, and the azimuth and elevation beamwidths 7° EL × 2° AZ and 1.3° EL × 40° AZ respectively, were simulated by their corresponding ultrasonic transducer beams. The scanning rate for the azimuth and elevation beams was 1.75 degrees/second. The results were adjusted for full-scale maximum sinusoidal scan rates of 691° and 377°/sec for AZ and EL respectively. The rain drops were simulated by air bubbles, with a similar size distribution, in water. The rain volume was created along a part of the propagation path, and not on the runway, because it was found difficult to avoid an accumulation of bubbles on the runway surface and surroundings simulated by the model surface.

The following are a summary of the results of the work reported in this final report:

1. No-rain multipath was found to occur in front of the azimuth and elevation transmitters, as was the case in NASA aircraft flight tests at Edwards AFB in California.

2. The ground multipath seen by the actual 50° EL × 80° AZ shuttle receiver coverage antenna is expected to be larger in amplitude than that measured by its simulated narrow beam antenna used

aboard the test aircraft in flight tests at Edwards AFB, California, based on ultrasonic simulated results.

3. All the multipath seems to occur at points on or in the immediate vicinity of the runway, and therefore the surrounding terrain does not contribute to multipath conditions for ranges up to 20,000 ft.

4. Since the multipath reflections from the runway and its immediate vicinity occur at angles less than or around 16 degrees from the azimuth, the reflection coefficient for vertical and horizontal polarization are within 3 db for this range of grazing angles and therefore ultrasonic simulation of MSBLS is valid.

5. The ultrasonically simulated multipath causes a -4 db beam center shift (caused by the very presence of runway as opposed to free space propagation between Orbiter and Azimuth scan transmitter) ranging from a minimum of 0.083 to a maximum of 0.625 degrees when referred to the free-space condition case. A similar shift is expected for the case of elevation scan.

6. The presence of simulated severe rain causes a further -4 db beam center shift by up to a maximum of 0.08° at 27,250 ft. range for azimuth scan, and 0.13° at 32,000 ft. range for elevation scan. The angular positioning accuracy of WPL - UH system is ± 0.01,° whereas range and altitude settings were within ± 8 feet of the full scale value.

7. Chase aircraft in different positions around the shuttle seemed to produce no degradation of the received beam shape.

It is further recommended that:

a. a cross correlation between full-scale beam center shift data and data obtained by ultrasonic simulation be obtained,

b. rain effects on the Orbiter received beamwidth be measured and analyzed in a test at Kennedy Space Center with MSBLS, so that rain-caused errors, if any, are clearly separated from the no-rain multipath conditions and

c. that cross-correlation be calculated between rain-caused multipath effects obtained for full-scale and ultrasonically simulated cases.

4. MSBLS DESCRIPTION AND IT'S ULTRASONIC/MODEL

The Orbiter MSBLS system modeling consisted of three separate tasks namely the azimuth and elevation scan transmitter as well as Orbiter receiver beamwidths, the geometry, and the runway and associated terrain. Each of these areas are discussed below in addition to polarization and signal waveform.

BEAMWIDTHS OF TRANSMITTERS AND RECEIVER

A summary of beamwidths of the azimuth and elevation scan transmitters as well as the Orbiter receiver are given in Table 4.1, and the corresponding beamwidth transducers are used in the ultrasonic model. One half inch diameter cylindrical disc transducers with specially constructed lenses were used to simulate these beamwidths. The Orbiter receiver coverage was simulated by 80° × 50° (AZ×EL) transducer whose two diagonal patterns/cuts are shown in Fig. 4.1. This unit satisfies the 4 db/8° period ripple and beamwidth requirements. This was the most difficult beam pattern to design, since procurement of an exact 80° × 50° pattern requirement would have been prohibitive in cost and time, and therefore this was considered to be the optimum from cost and delivery time standpoints. Since the Orbiter receiver coverage shows a considerable ripple therefore its transducer coverage representing it is probably as good a fit as one can achieve in practice.

The 40° × 1.3° (AZ×EL) elevation scan transmitter was simulated by its corresponding transducer (XDCR) with both pattern cuts shown in Fig. 4.2, whereas the 2° × 7° (AZ×EL) azimuth scan transmitter counterpart transducer patterns are shown in Fig. 4.3. A close examination of these two coverages shows that these approximated the full-scale antenna patterns.

Thus having approximated the beamwidth of the antennas, one comes to the scan rates. The maximum full-scale sinusoidal EL and AZ scan rates were approximately 377° and 691°/second respectively, and such rates are well nigh impossible to duplicate in a water tank for a variety of reasons. Thus, practicality of slow scan rate, necessitated by the requirement of disturbing the propagation medium (water), of the order of 1.75° per second were used. The effect of slow scan rates is to preserve the high-frequency time variations of the signal, whereas the high scan rates would tend to act as lowpass filter which filters out such high frequency content and smooths out the waveform distortion. This, when translated in terms of the Orbiter received beam-shape, means that any distortion of the said beam-shape will be smoothed out but the basic "dent" shall remain, or in other words frequencies of the order up to 215 and 395 times for EL and AZ respectively would be filtered. This point is also discussed in the chapter on rain simulation and discussion of results and therefore no further details are provided in this chapter.

LANDING TRAJECTORY AND GEOMETRY OF TRANSMITTERS/RECEIVER

During the first phase of this work, it was mutually decided to select points on the Orbiter landing trajectory provided by NASA, and to statically simulate the received signal beam-shape for analysis of the effects of the ground multipath. The location of the elevation and azimuth scanning transmitters and a summary of their beamwidths and orientations are shown in Fig. 4.4. In each of these figures, model distances calculated using linear wavelength scaling are also shown (See Table 4.1 and Chapter 5). Linear wavelength scaling preserves the phase and amplitude effects exactly except for a fixed db shift between the electromagnetic and ultrasonic received signal levels.

In the case of the Orbiter trajectory, it was essential that both the elevation and range as well tilt angle of the receiver with respect to transmitters be maintained exactly the same as in the full scale electromagnetic case. Therefore, in order to simulate exactly the ground multipath, one uses a simple geometry shown in Fig. 4.4 in order to arrive at a range scale factor of 3200:1 and an elevation scale factor of 3310:1. Based on these scale factors, and the actual grazing angles of multipath, one calculates the corresponding range and elevation for the trajectory in the water for the ultrasonic model. The results of such a calculation are shown in Fig. 4.5 where range, elevation, beam depression angle are listed for both the full-scale electromagnetic as well as for the ultrasonic model case.

POLARIZATION AND SIGNAL WAVE FORM

Since MSBLS uses vertical polarization and that the grazing angles of the order of or less than 16° are involved in the ground multipath mode, it is not unreasonable to expect a difference of two to three db in the reflection coefficients for vertical and horizontal polarization when one combines the phase and amplitude effects of the surface roughness. As the ground roughness decreases or it becomes a better conductor, the differences between amplitudes for two polarizations reduce to negligible proportions (see Chapter 5) for such small grazing angles. This is even much more valid for rain conditions, since water cannot support shear (lateral) waves, longitudinal (compressional) waves are used to simulate the vertical polarization. Further details on this matter are provided in Chapter 5, with examples.

Continuous sine wave signals was transmitted and received in the ultrasonic model system, and the other details of the experimental system are given in Chapter 6.

OTHER FACTORS AND RUNWAY MODEL

Chase planes were simulated by 1/72th scale commercially available jet aircraft coated with appropriate aluminum-zinc loaded epoxy in order to guarantee appropriate Fresnel reflection coefficient.

The runway was constructed of lucite-air-lucite sandwich which was completely air-sealed. The Fresnel reflection coefficient of the smooth surface was found to match that of paved runway or a lake bed so well in the 0-30° grazing angle range that this construction was preferred over our classical built-up models used successfully in the past decades. Photographs of the deck are shown in Chapter 6.

The area surrounding the runway was buffed to make it appear rough for 2.25 megahertz ultrasonic waves used in the model experiment based on $\lambda/10$ roughness criterion for vertical incidence (Hayre 1962). A general reflection coefficient check of the model runway and the surrounding area were verified before the final tests were run in the model experiment.

The following symbols are used in Table 4 following this page:

L = Length

f_a = frequency in air (actual frequency)

f_w = frequency in water (model frequency)

R = Range scale factor

c_a, c_w = velocity of wave propagation in air, in water

λ_a λ_w = wavelengths in air and water

Subscript a = for air

w = for water

TABLE 4.1 FULLSCALE AND MODEL MSBLS PARAMETERS

	FULLSCALE ORBITER	ULTRASONIC MODEL
1(a)	Length = L = 1467.06"	50.76"
	Wing Span = 936.68	32.4"
	Height Stab. Tip = 679"	23.5"
	f_a = 15.4 - 15.7 GHZ	Ultrasonic wave velocity
	Center f_a = 15.55 GHZ	in water = $c_w = 1.5 \times 10^3$ m/sec
	$C_a = 3 \times 10^8$ m/sec	Ultrasonic frequency f_w = ?

WAVELENGTH SCALE FACTOR (R)

$R = \lambda_a/\lambda_w = (Ca/Cw) \cdot (fw/fa) = 28.938 \simeq 29$

$L \sim 48" \rightarrow 50" \rightarrow R \simeq 29$ $\qquad f_w = 2.25$ MHZ

Wing Span $\sim 24" \rightarrow 36"$

1(b) MSBLS ANTENNA/RADAR SIMULATION

Elevation Beam 1.3° EL × 40° AZ (-3 db) (0-30° EL. SCAN.)

side lobe -18 db

Azimuthal Beam 7° EL × 2° AZ (-3 db) ± 15° scan in AZ)

side lobe -20 db

SHUTTLE MSBLS RECEIVER ANTENNA

$-40° \leq \phi \leq +40°, \quad -23° \leq \Theta \leq +27°$

Ripple 4 db ma/8° period

Gain grad.: a maximum of 0.5 db/degree

Ultrasonic Beams Identical
Transducer 1/2"; 2.25 MHZ, Special Lenz

1(c) Controlled Azimuth and Vertical Scan Using Flexible Shaft/Scientific Atlanta Positioner

Position Accuracy - 0.01°

1(d) Polarization - Vertical ------ (Longitudinal Waves)

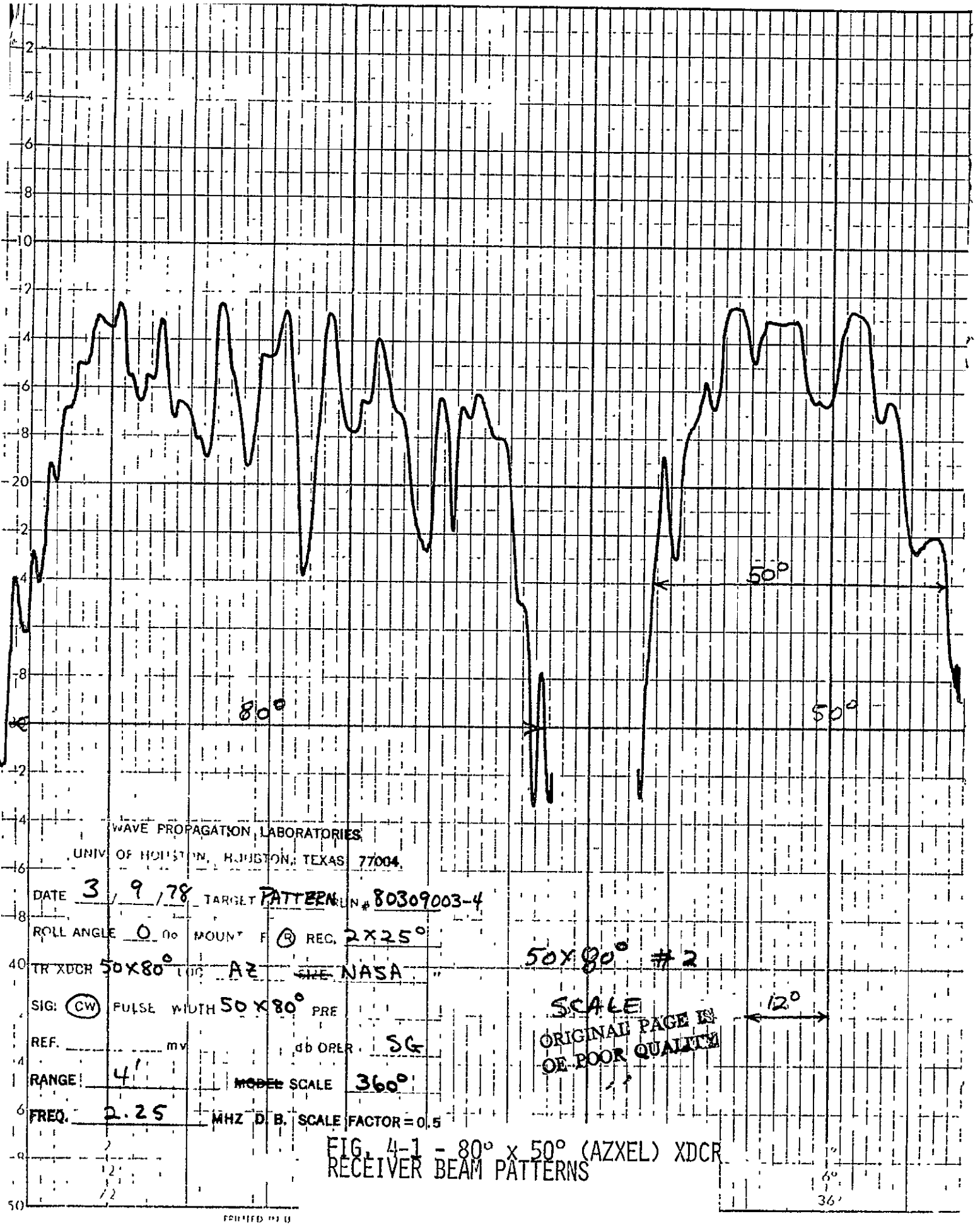

FIG. 4-1 - 80° x 50° (AZXEL) XDCR RECEIVER BEAM PATTERNS

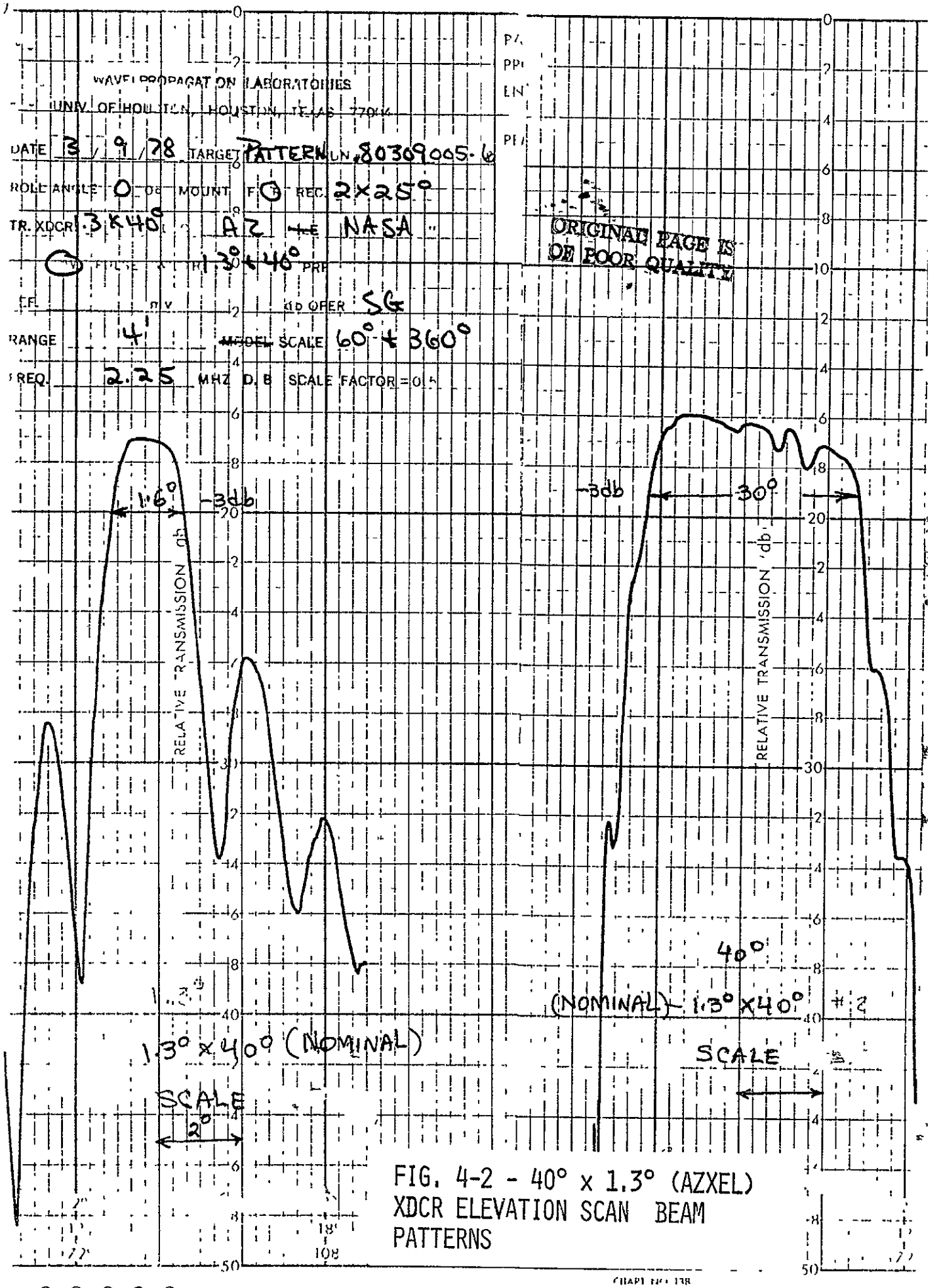

FIG. 4-2 - 40° x 1.3° (AZXEL) XDCR ELEVATION SCAN BEAM PATTERNS

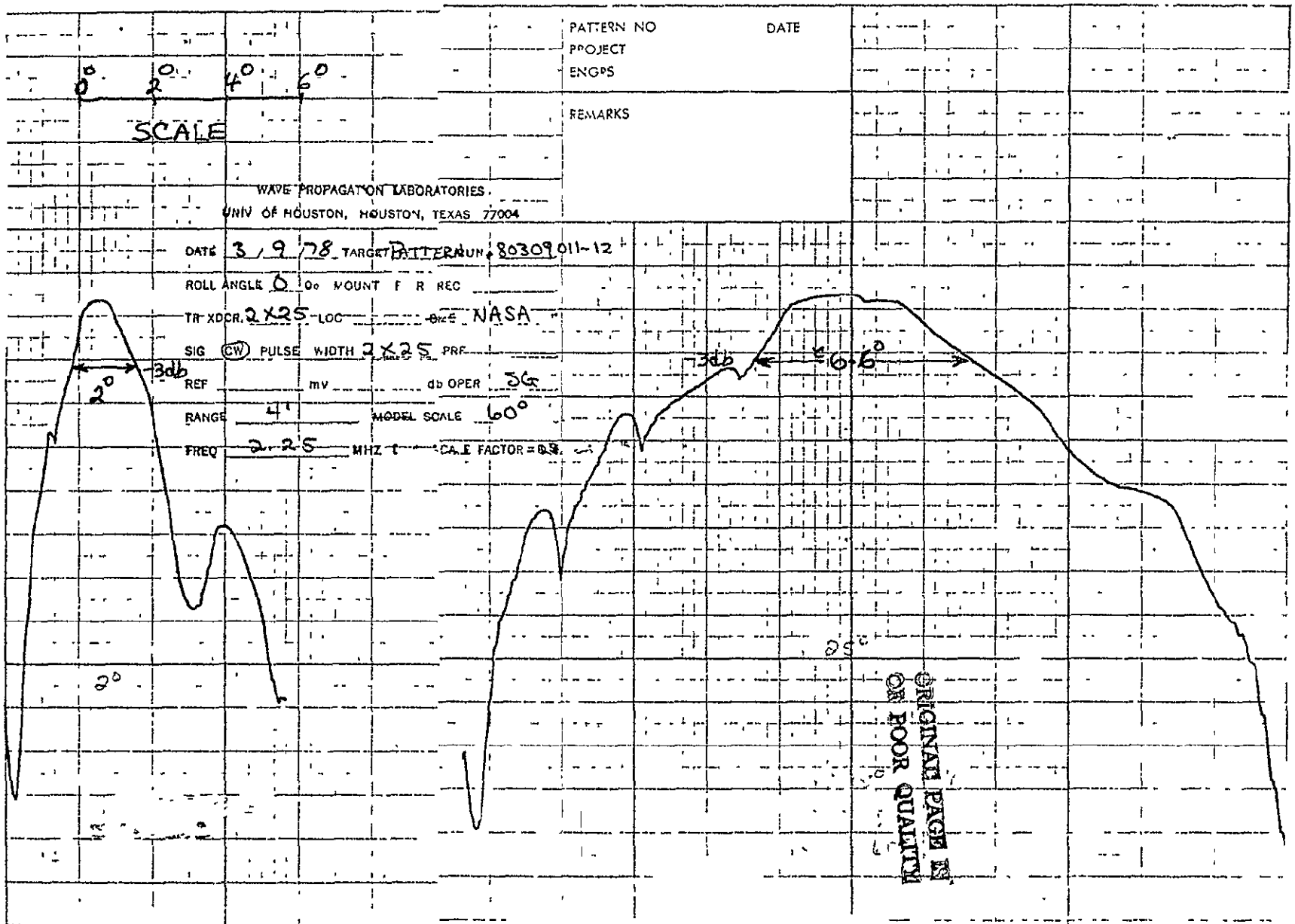

FIG. 4-3 - 2° x 7° (AZXEL) XDCR" AZIMUTHAL SCAN BEAM PATTERNS

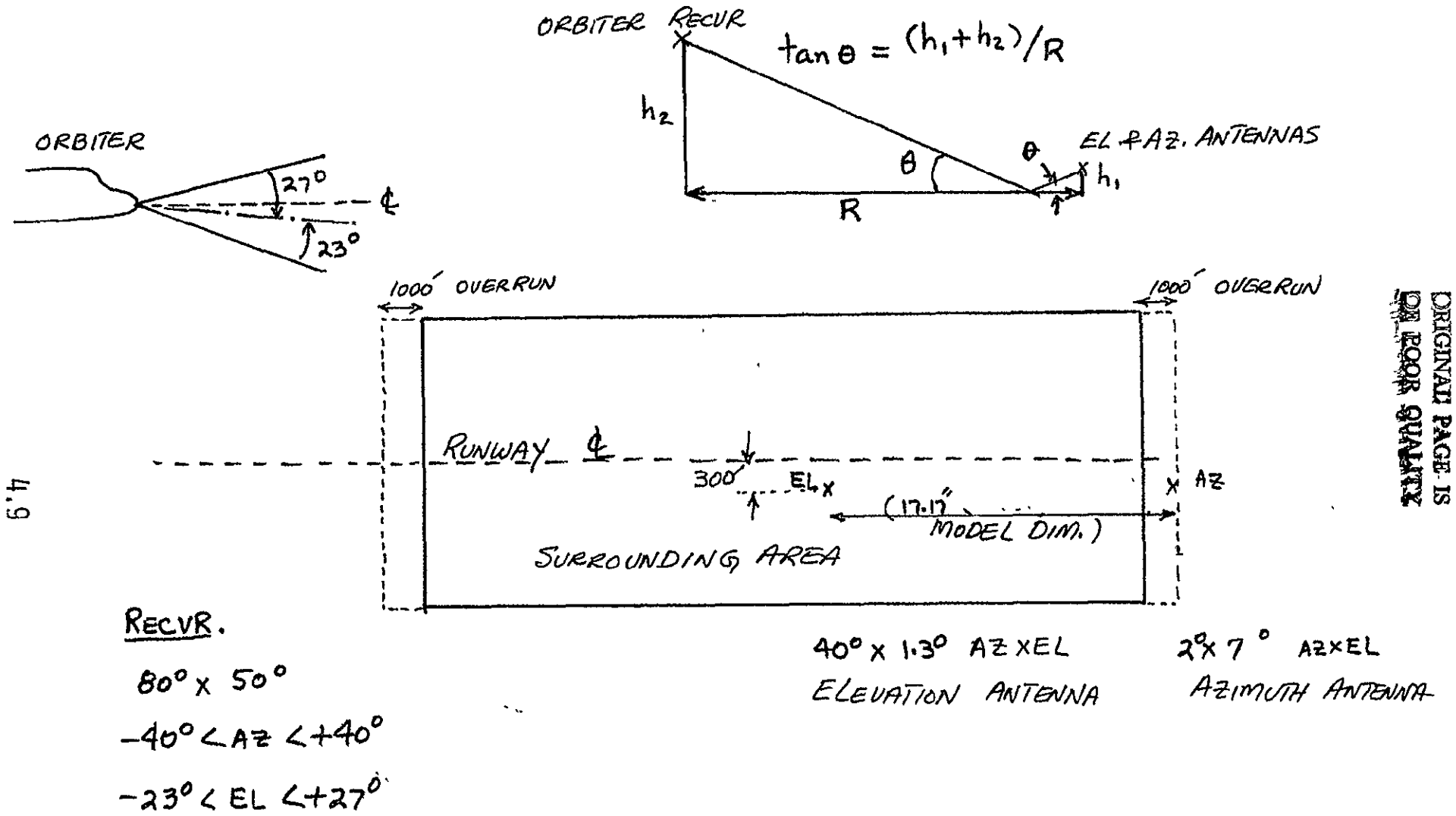

FIG. 4.4 ORBITER MSBLS RUNWAY CONFIGURATION

FIG.-4.5 NASA-MSBLS

SIMULATED RANGE/ ALTITUDE /BEAM DEPRESSION ANGLE

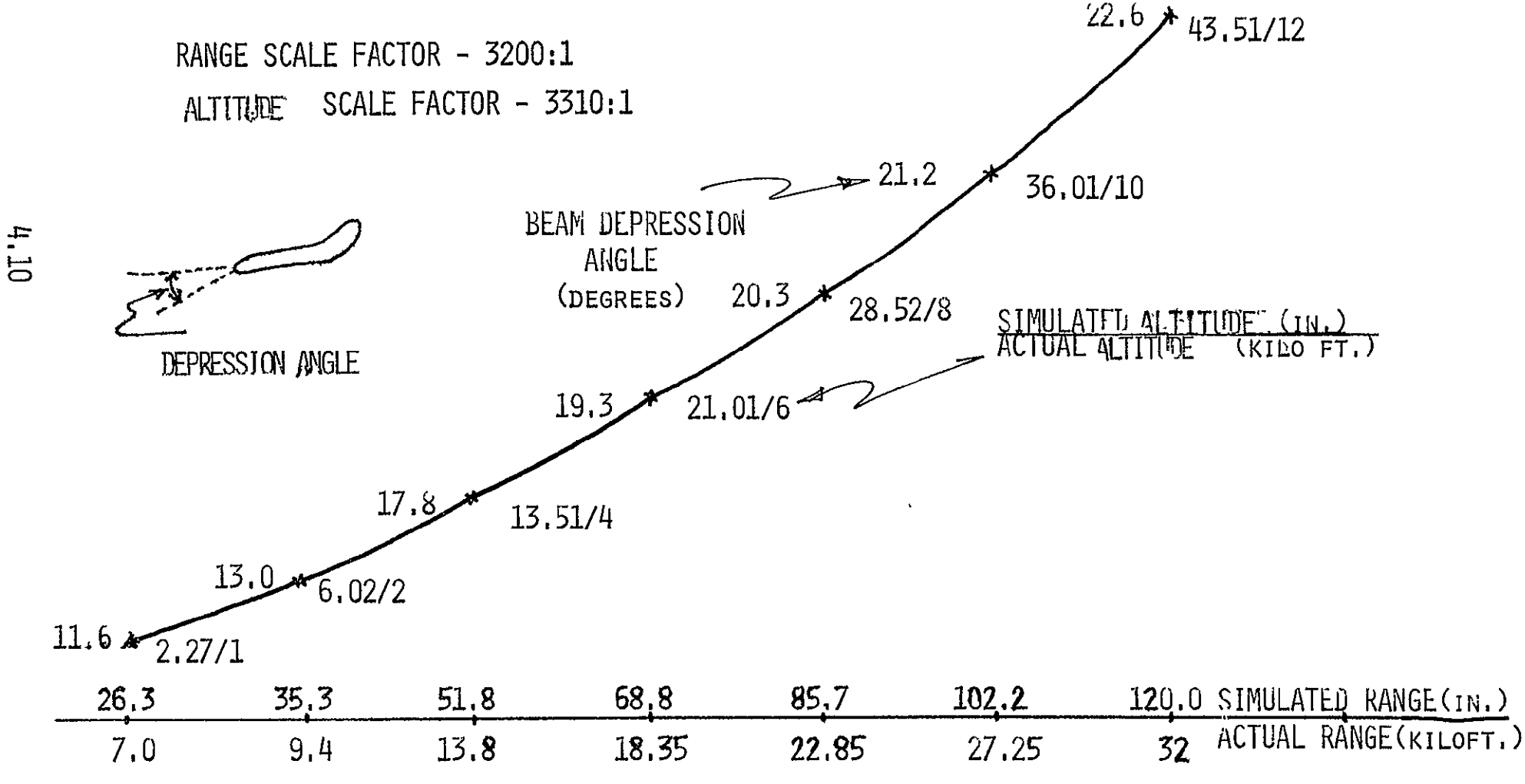

4.10

5. VERTICAL POLARIZATION MSBLS MULTIPATH AND ITS ULTRASONIC SIMULATION

In case of acoustic waves in water, there is no polarization, and the pressure wave P is longitudinal. The associated particle velocity $\overline{U}$ is always along the direction of propagation. It will be shown later that the pressure wave P is an exactly analog of the E_H type polarization. Since liquids cannot support transverse waves, there is no parameter exactly analogous to E_V polarization in electromagnetics, except for airframe mounted antenna, near-grazing and near-vertical incidence cases, and for the case of almost perfectly conducting surfaces.

WAVE EQUATION

The wave equation for a uniform plane electromagnetic wave in free space and acoustic wave in water are analogous (Morse, 1968):

E. M. Waves (Air)	Acoustic Waves (Water)	
$\nabla^2\overline{E} = \mu\varepsilon \frac{\partial^2\overline{E}}{\partial t^2}$	$\nabla^2\overline{U} = \rho K \frac{\partial^2\overline{U}}{\partial t^2}$	(5-1)
$\nabla^2\overline{H} = \mu\varepsilon \frac{\partial^2\overline{H}}{\partial t}$	$\nabla^2 P = \rho K \frac{\partial^2 P}{\partial t^2}$	(5-2)

where: $\overline{E}$ = Electric field intensity vector, (volts/m)

$\overline{H}$ = Magnetic field intensity vector, (amp/m)

$\overline{P}$ = Scalar pressure field, (N/m^2)

$\overline{U}$ = Particle velocity vector, (m/sec)

ρ = Density of medium, (kg/m^3)

k = Compressibility of medium, (m^2/N)

ε = Permittivity of medium, (f/m)

μ = Permeability of medium, (h/m)

Assuming e^{jwt} variation for both systems, solutions to the above cases of uniform plane waves propagating in negative z-direction are: (Kraus, 1973)

Electromagnetic	Acoustic	
$\overline{E}_x = \overline{E}_0 e^{j(wt+kz)}$	$P_z = P_0 e^{j(wt+kz)}$	(5-3)
$\overline{H}_y = \overline{H}_0 e^{j(wt+kz)}$	$\overline{U}_x = \overline{U}_0 e^{j(wt+kz)}$	(5-4)

Since these forms of the solutions are identical, and differ only by the physical constants in the respective systems, therefore one concludes that there is an exact analogy between these two systems.

BOUNDARY CONDITIONS

Boundary conditions in electromagnetic case require that tangential components of $\overline{E}$ and $\overline{H}$ are continuous across the boundary; i.e.

$$\overline{n} \times (\overline{E}_1 - \overline{E}_2) = 0 \tag{5-5}$$

$$\overline{n} \times (\overline{H}_1 - \overline{H}_2) = 0 \tag{5-6}$$

For the acoustic case, the pressure P and normal component of particle velocity $\overline{U}$ are also continuous across the interface between the two media: (See Fig. 5.5)

$$P_1 = P_2 = P \tag{5-7}$$

$$\overline{n} \cdot (\overline{U}_2 - \overline{U}_1) = 0 \tag{5-8}$$

Boundary condition at a perfect conductor require the tangential electric field to be zero, and the tangential magnetic field to be two times the incident field. On the other hand, at a perfectly elastic wall, the dynamic

acoustic pressure is zero and the normal component of the total particle velocity is twice the normal component of the incident particle velocity. In each of the situations there is no wave propagation beyond the interface.

It has been well established, that specially constructed acoustic models with air-backed surfaces behave exactly like air/aluminum or air/steel interfaces or air/good conducting ground or pavement for electromagnetic waves in so far as the Fresnel Reflection Coefficient are concerned. (See Fig. 5-1). This is also valid for NASA shuttle runway simulated by lucite-air-lucite sandwich.

REFLECTION COEFFICIENT

If a vertically polarized electric field vector is incident on a smooth surface in x-z plane at an angle θ_1 along the vector, $\bar{A}_k$ and is partially specularly reflected into the same dielectric medium and partially transmitted into the second medium at an angle θ_2 as shown in Figure 5-2, then reflection coefficient R_V is,

$$R_V = \frac{Z_2' - Z_1'}{Z_2' + Z_1'} \tag{5-9}$$

whereas its transmission coefficient, T_V is,

$$T_V = \frac{2Z_2'}{Z_1' + Z_2'} \left(\frac{\text{Cos } \theta_1}{\text{Cos } \theta_2}\right) \tag{5-10}$$

where: $$Z_2' = \left(\frac{\mu_2}{\varepsilon_2}\right)^{1/2} \text{Cos } \theta_2 \tag{5-11}$$

$$Z_1' = \left(\frac{\mu_1}{\varepsilon_1}\right)^{1/2} \text{Cos } \theta_1 \tag{5-12}$$

In the case of horizontal polarization, the reflection and transmission coefficient for a plane interface between two infinite dielectric slabs are, (See Fig. 5.3)

$$R_H = \frac{Z_2'' - Z_1''}{Z_2'' + Z_1''} \tag{5-13}$$

$$T_H = \frac{2Z_2''}{Z_1'' + Z_2''} \tag{5-14}$$

where: $$Z_2'' = \left(\frac{\mu_2}{\varepsilon_2}\right)^{1/2} \text{Sec } \theta_2 \tag{5-15}$$

$$Z_1'' = \left(\frac{\mu_1}{\varepsilon_1}\right)^{1/2} \text{Sec } \theta_1 \tag{5-16}$$

An acoustic wave incident in water on a solid surface splits into two parts; longitudinal and shear waves in the solid medium (see Figure 5-4). The equivalent impedance of medium 1 and 2 are given (Brekhovskikh, 1960) as,

Impedance: Longitudinal, $$Z_{\ell i} = \rho_i C_i \text{ Sec } \theta_i \tag{5-17}$$

Transverse, $$Z_t = \rho_2 b_2 \text{ Sec } \nu_2 \tag{5-18}$$

Longitudinal: Reflection coefficient,

$$R_1 = \frac{Z_{total} - Z_1}{Z_{total} + Z_1} \tag{5-19}$$

Transmission coefficient,

$$T_1 = \frac{\rho_1}{\rho_2} \cdot \frac{2(Z_2 \cos 2\nu_2)}{Z_{total} + Z_{\ell 1}} \tag{5-20}$$

Transverse Transmission coefficient,

$$T_{sh} = \frac{\rho_1}{\rho_2} \frac{2(Z_t \cos \nu_2)}{Z_{total} + Z_{\ell 1}} \tag{5-21}$$

where: $b^2 = \frac{\mu}{\rho}$ = Shear velocity (5-22)

$C^2 = \frac{\lambda+2\mu}{\rho}$ μ = Lame's Constant (5-23)

$$Z_{total} = Z_2 \cos^2 2\nu_2 + Z_t \sin^2 2\nu_2 \quad (5\text{-}24)$$

THEORY FOR SIMULATION OF VERTICAL AND HORIZONTAL POLARIZATION

The Fresnel reflection coefficients for vertically and horizontally polarized electromagnetic waves at a boundary between two dielectric media are given as (Stratton, 1941)

$$R_H = \frac{\mu_2 k_1 \text{Cos } \theta_1 - \mu_1 k_2 \text{Cos } \theta_2}{\mu_2 k_1 \text{Cos } \theta_1 + \mu_1 k_2 \text{Cos } \theta_2} \quad (5\text{-}25)$$

$$R_V = \frac{\mu_2 k_1 \text{Cos } \theta_2 - \mu_1 k_2 \text{Cos } \theta_1}{\mu_2 k_1 \text{Cos } \theta_2 + \mu_1 k_2 \text{Cos } \theta_1} \quad (5\text{-}26)$$

where θ_1 and θ_2 are angles of incidence and transmission respectively as shown in Fig. 5-2. The presence of conductivity in one of the medium modifies the reflection coefficient.

If medium (1) is a perfect dielectric and medium (2) is conducting, then the propagation constants are defined as

$$k_1 = \alpha_1 = w\sqrt{\mu_1 \varepsilon_1} \quad (5\text{-}27)$$

$$k_2 = \alpha_2 + j\beta_2 \quad (5\text{-}28)$$

where α is the phase constant and β is the attenuation factor.

For a dielectric/conducting interface, the Snell's law is modified as given below:

$$k_1 \text{ Sin } \theta_1 = k_2 \text{ Sin } \theta_2 \tag{5-29}$$

$$\text{Sin } \theta_2 = \frac{k_1}{k_2} \text{ Sin } \theta_1 = \frac{\alpha_1}{\alpha_2^2 + \beta_2^2} (\alpha_2 - j\beta_2) \text{ Sin } \theta_1 \tag{5-30}$$

The above equation can be rewritten in a convenient form, given below:

$$\text{Sin } \theta_2 = (a - jb) \text{ Sin } \theta_1 \tag{5-31}$$

The Cos θ_2 becomes a complex quantity as defined below:

$$\text{Cos } \theta_2 = \sqrt{1-(a^2-b^2-i\ 2ab)\ \text{Sin}^2\theta_1}\ \ Pe^{j\nu} \tag{5-32}$$

Then an application of the Snell's law yields:

$$k_2 \text{Cos } \theta_2 = \sqrt{k_2^2 - k_2^2\ \text{Sin}^2\theta_2} = \sqrt{k_2^2 - k_1^2\ \text{Sin}^2\theta_1} \tag{5-33}$$

Now substituting Eq. (5-33) in Eq. (5-25) and Eq. (5-26), one obtains, (Stratton, 1941), the following:

$$R_H = \left[\frac{(\alpha_2 - \alpha_1 \text{Cos } \theta_1)^2 + \beta_2^2}{(\alpha_2 + \alpha_1 \text{Cos } \theta_1)^2 + \beta_2^2}\right]^{1/2} e^{j\delta_H} \tag{5-34}$$

$$R_V = \left[\frac{[(\alpha_2^2-\beta_2^2)\text{Cos } \theta_1 - \alpha_1\alpha_2]^2 + [2\alpha_2\beta_2 \text{Cos } \theta_1 - \alpha_1\beta_2^2]^2}{[(\alpha_2^2-\beta_2^2)\text{Cos } \theta_1 + \alpha_1\alpha_2]^2 + [2\alpha_2\beta_2 \text{Cos } \theta_1 + \alpha_1\beta_2^2]^2}\right]^{1/2} e^{j\delta_V} \tag{5-35}$$

In case of a conductor,

$$\eta_2^2 = \frac{\sigma_2^2}{w^2\varepsilon_2^2} \gg 1 \tag{5-36}$$

and

$$\alpha_2 = \beta_2 \simeq \sqrt{\frac{w\mu_2\sigma_2}{2}} \tag{5-37}$$

therefore R_H and R_V become, (Stratton, 1941),

$$|R_H|^2 \simeq \frac{(1-\frac{\mu_2\alpha_1}{\mu_1\alpha_2}\,\mathrm{Cos}\,\theta_1)^2+1}{(1+\frac{\mu_1\alpha_2}{\mu_1\alpha_2}\,\mathrm{Cos}\,\theta_1)^2+1} \tag{5-38}$$

$$|R_V|^2 \simeq [x^2+(2\mathrm{Cos}\theta_1-x_2)^2]/[x^2+(2\mathrm{Cos}\theta_1+x)^2] \tag{5-39}$$

Since in case of all conductors $\frac{\mu_2\alpha_1}{\mu_1\alpha_2} << 1$, and denoting the quantity $\frac{\mu_2\alpha_1}{\mu_1\alpha_2}$ by x, one can rewrite (5-39) as below:

$$|R_H|^2 \simeq 1 - 2x\,\mathrm{Cos}\,\theta_1 \tag{5-40}$$

Similarly the reflection coefficient for vertical polarization, can be simplified to the following form:

$$|R_V|^2 = \frac{2\mathrm{Cos}^2\,\theta_1 - 2x\mathrm{Cos}\,\theta_1 + x^2}{2\mathrm{Cos}^2\,\theta_1 + 2x\mathrm{Cos}\,\theta_1 + x^2} \tag{5-41}$$

At normal incidence ($\theta_1 = 0°$), $|R_H| = 1 - 2x$ (5-42)

and $$|R_V|^2 = \frac{2 - 2x + x^2}{2 + 2x + x^2} \tag{5-43}$$

$$|R_V|^2 = \frac{(1 - x)^2 + 1}{(1 + x)^2 + 1} \tag{5-44}$$

Applying binomial theorem to Eq. (5-39), $|R_V|$ reduces to

$$|R_V|^2 = 1 - 2x \tag{5-45}$$

which is the same as Eq. (5-42) for perpendicular polarization. For grazing incidence ($\theta \simeq 90°$), one obtains

$$|R_H|^2 = |R_V|^2 = 1 \tag{5-46}$$

For near-vertical and near grazing angles, magnitudes of R_H and R_V are equal, and the range of angles in these two cases depends on the specific conducting material (depends on x). Brekhovskikh, (1960) and Stratton, (1941) present plots of R_V and R_H from 0° to 90° angles for different interfaces.

A sample calculation of R_V and R_H for air/aluminum interface (typical of air frame mounted antennas) for a range of incidence angles from 0° to 90° is given next. The value of x for non-magnetic materials is given by

$$x = \frac{\mu_1\alpha_1}{\mu_2\alpha_2} \simeq \frac{\alpha_1}{\alpha_2} \tag{5-47}$$

The phase constant of E.M. wave in air, ($\alpha_1 = w\sqrt{\mu_1\varepsilon_1}$) for

$$\omega = 10^9 \times 2\pi(5\rightarrow10) \text{ rps}$$

$$\mu = 1.25 \times 10^{-6} \text{ h/m}$$

$$\varepsilon_1 = 8.84 \times 10^{-12} \text{ f/m}$$

$$\therefore \alpha_1 = 104.35 \rightarrow 108.70$$

The phase constant of E.M. wave in aluminum,

$$\omega = 2\pi \times (5\rightarrow10) \times 10^9 \text{ rps}$$

$$\mu_2 = 1.25 \times 10^{-6} \text{ h/m}$$

$$\sigma_2 = 3.5 \times 10^7 \text{ mho/m}$$

$$\therefore \alpha_2 = 146.92 \rightarrow 293.84$$

$$\therefore \quad x = \frac{\alpha_1}{\alpha_2} = 0.71 \times 10 \times 10^{-4}$$

Similarly for steel $x = 0.122 \rightarrow 0.174$

efficient for the longitudinal waves from the model surfaces is also essentially constant near the near-normal and near-the-grazing angle domains for the angles of incidence encountered in MLS and in MSBLS multipath geometries.

The basic angles of incidence for MSBLS case for the range of altitudes considered here is approximately 70° to 82°, when measured from the outward normal. Since the sandy dry lake runway at Edwards may be said to have relative dielectric constant ε_r = 10 f/m, and the conductivity of approximately 2×10^{-3} mhos per meter, therefore the lake bed and the metal runways both at Edwards AFB and Kennedy Space Center, under rain condition would somewhat behave like a material midway between a fresh water surface and the moist sandy surface. Since fresh water has an ε_r = 75, and its conductivity may vary from 1 to 20 mhos/m, it is reasonable to assume an average value of 10 for the conductivity.

Now, for an ideal smooth surface at 15 GHz, the Fresnel reflection coefficients has been measured for a smooth sandy surface to be, for $70° < \theta < 82°$

$$0.8 < R_H < 0.91$$

$$0.2 < R_V < 0.4$$

and for smooth fresh water surface to be

$$0.83 < R_H < 0.97$$

$$0.5 < R_V < 0.1$$

Under actual operating conditions, MSBLS microwave radiation would encounter a fairly rough surface in case of the dry lake bed, and, also under rainfall conditions in case of both the metal runways and the lake bed.

From extensive experience in scattering from random rough surfaces, it may be stated that 0.2 - 0.4 and 0.5 - 0.1 variations would considerably be smoothed out and one may expect the range of R_V to be within one to two dbs at the maximum. This condition is confirmed by the reflection coefficient variation for the model surface (shown in Fig. 5.1) of approximately 0.5 - 0.75 db for $70° < \theta_i < 82°$. Therefore it is concluded that the special surface of water/air backed plexiglas (sandwich) interface simulates all MSBLS runway conditions reasonably well.

For instance, most of the multipah from the runway comes from near-grazing incidence, and primarily the worst case is caused by strong specular reflections in the direction of the approaching shuttle, for which case

$$|R_V| \simeq |R_H| = |R_L| \qquad \text{for rough surfaces} \qquad (5\text{-}50)$$

where R_L = longitudinal acoustic wave reflection coefficient. In fact even if $|R_L|$ is not equal to $|R_V|$ and $|R_L|$, as shown in Figs. 5.1 and 5.7, but its variation over the range of angles of interest is relatively insignificant, then the fading pattern at the receiver aboard the landing craft is identical in shape to the full-scale electromagnetic case for either polarization. Of course the dynamic range of the fading shall be truly simulated by its ultrasonic model, and the amplitude of the simulated results would differ from the full scale by a constant factor, thus not affecting the -4 db beam centers used in this work.

In summary it has been shown that $|R_L|$ simulates horizontal polarization exactly and the vertical polarization for near grazing and near normal angles of incidence to an accuracy of ± 1-2 percent.

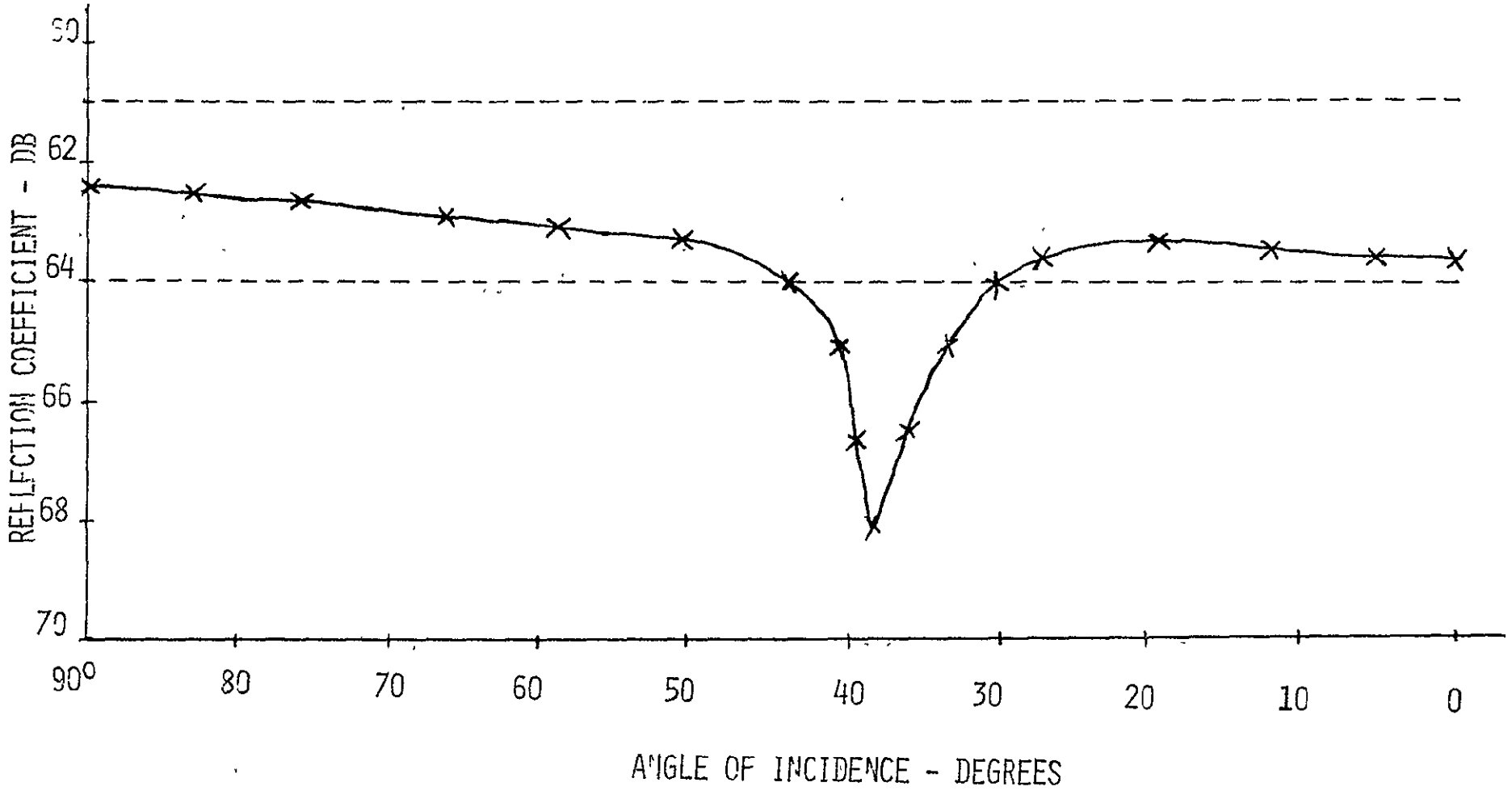

FIG. 5.1 ACOUSTIC REFLECTION COEFFICIENT VS ANGLE OF INCIDENCE FOR H_2O/AIR-BACKED PLEXIGLASS INTERFACE

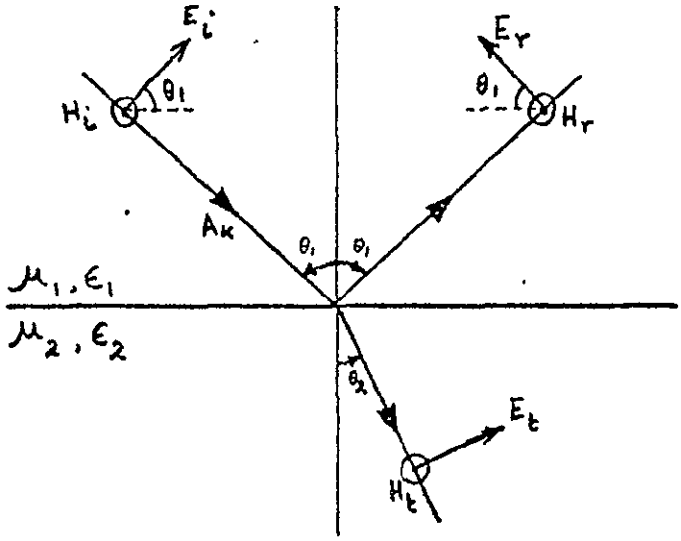

FIG. 5.2 REFLECTION AND TRANSMISSION OF VERTICALLY POLARIZED WAVE AT OBLIQUE INCIDENCE

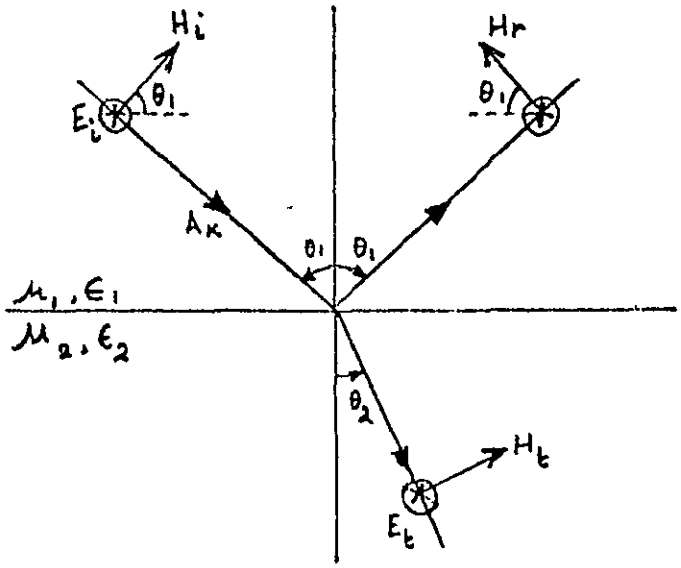

FIG. 5.3 REFLECTION AND TRANSMISSION OF HORIZONTALLY POLARIZED WAVE AT OBLIQUE INCIDENCE

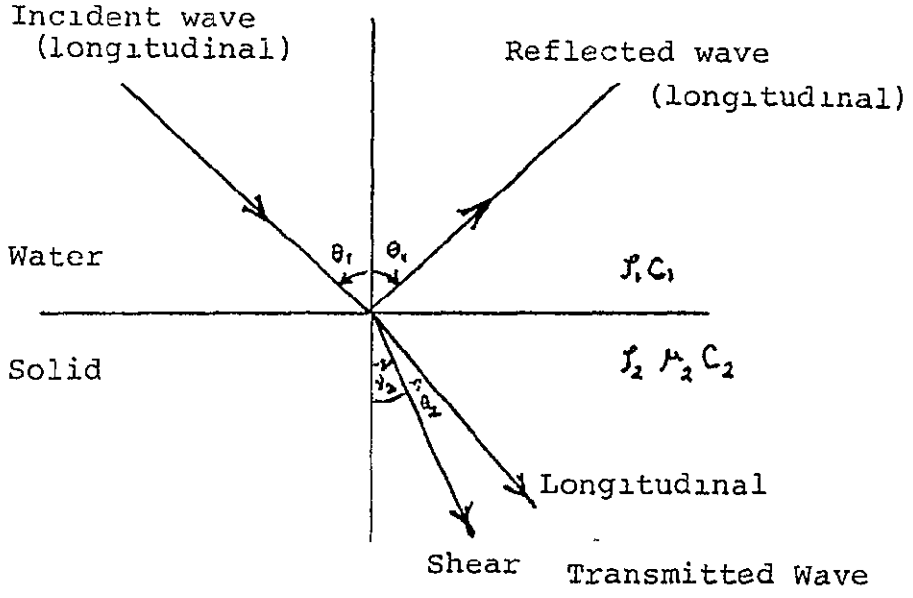

FIG. 5.4 REFLECTING AND TRANSMISSION OF LONGITUDINAL ACOUSTIC WAVE AT SOLID/WATER INTERFACE

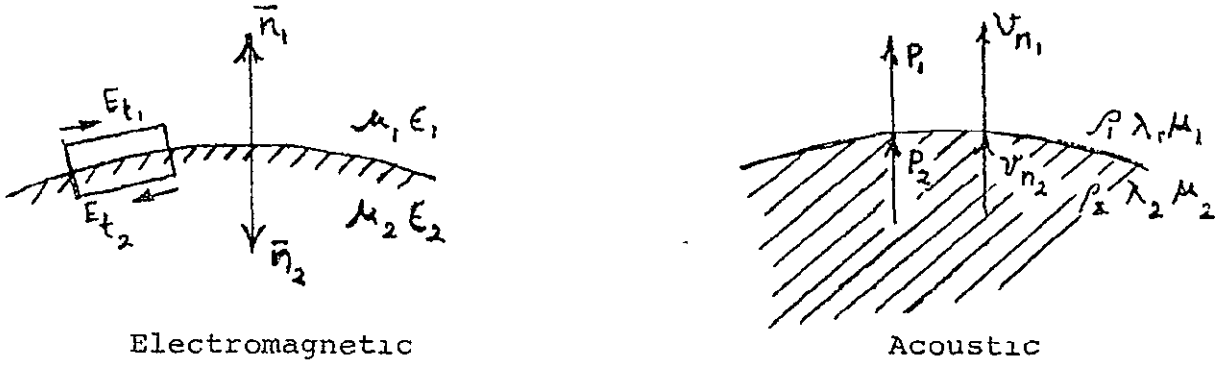

FIG. 5.5 BOUNDARY CONDITIONS AT AN INTERFACE FOR ELECTROMAGNETIC AND ACOUSTIC WAVES

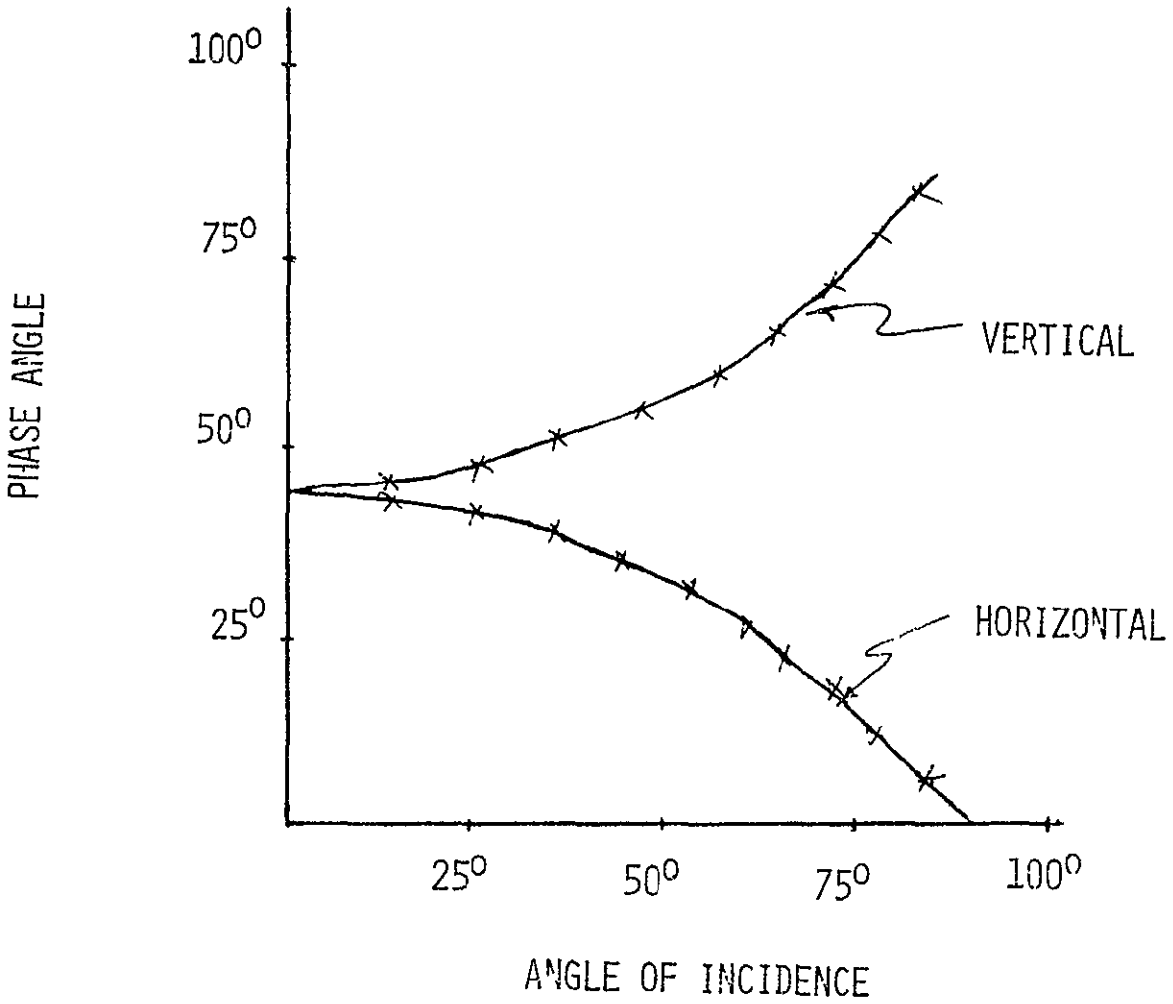

FIG. 5.6 RELATIVE PHASE ANGLE OF R_V, R_H VERSUS ANGLE OF INCIDENCE

FIG. 5.7 FRESNEL REFLECTION COEFFICIENT VS ANGLE OF INCIDENCE FOR AIR/WATER INTERFACE FOR (EMW) R_H &R_V AND ACOUSTICS

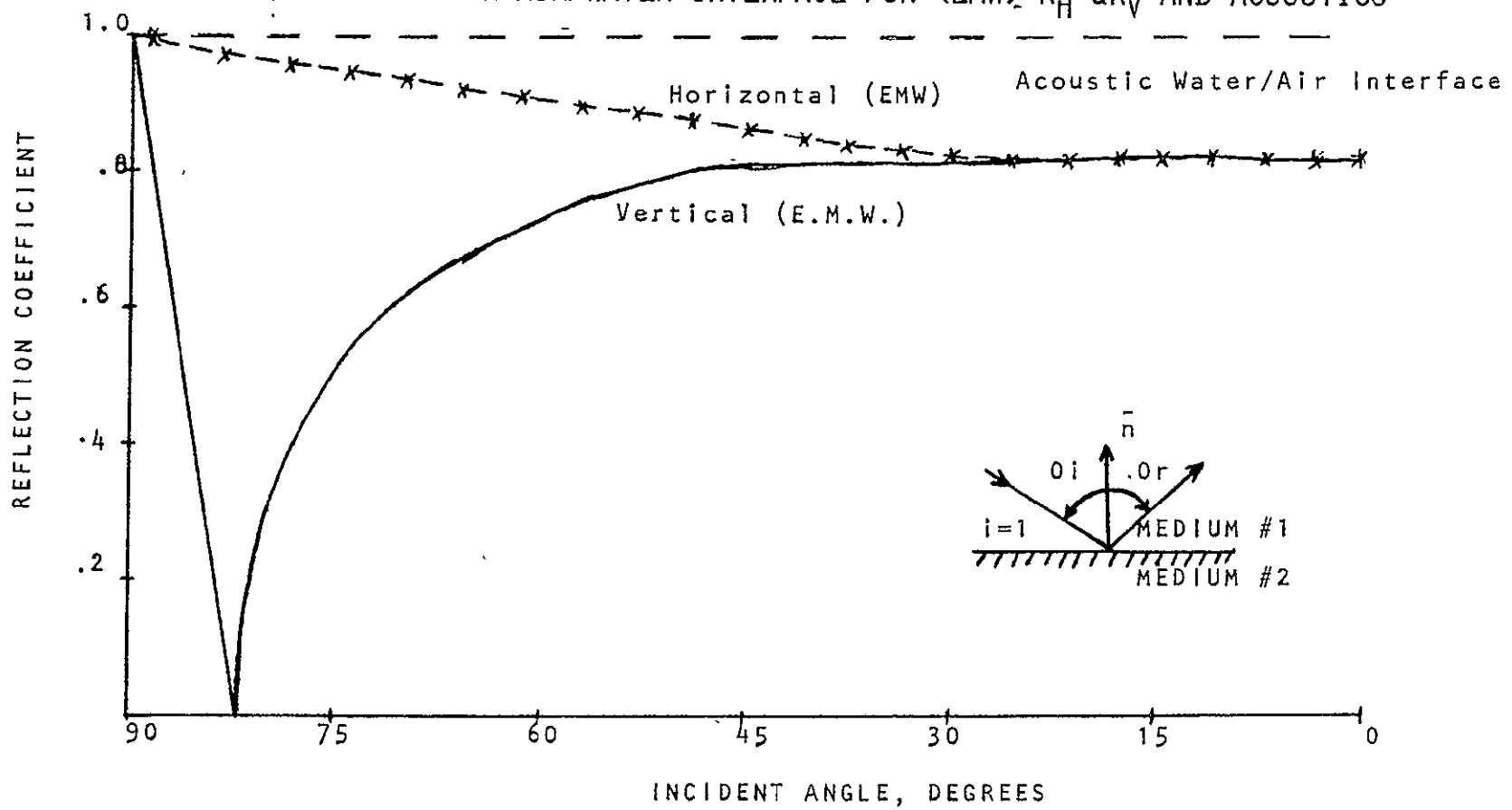

6. SIMULATION EXPERIMENTAL SETUP

Since in the ultrasonic simulation, the propagation media is water volume, and therefore the simulation experimental setup is a mirror image of the full scale setup, in that the 4' × 4' model runway shown in Fig. 6.1a is turned over such that the highest elevation point on the trajectory is the deepest point in water. Two detailed views of the whole setup are shown in Fig. 6.1b and c.

The ultrasonic frequency of 2.25 megahertz, as determined by linear wavelength scale modeling discussed in Chapter 4, is used to simulate the 15 gigahertz signal used in MSBLS. Since the receiver coverage on Orbiter was used to design the receiver transducer, only the receiver transducer, instead of the Orbiter model with the transducer mounted on it, is deployed.

A typical block diagram in Fig. 6.2 shows the electronic system. Either a 600 volt peak to peak Ahrenberg signal generator followed by an Ahrenberg tuner or a General Radio oscillator and HP 467A power amplifier are used to feed the azimuth and elevation scanning transmitters one at a time. The 93 ohm coaxial cable connecting the oscillator to the transmit transducer is approximately 65 feet long, therefore it was found necessary to use the high voltage Ahrenberg source, in particular for the farthest (120") trajectory point. The receiver transducer is mounted on a special L-frame (See Figs. 6.3 and 6.4) supported by cross and side braces in order to minimize its displacement in water and to dampen its motion. The vertical leg of the L-frame is mounted on the side of a carriage, which can travel on two parallel rails set up across the top of the 12 feet wide water tank. This two-rail system is mounted on an Otis elevator carriage which rides two rails mounted on the top of the two 42' long side tank walls. This enables the

operator to adjust the horizontal range as well as the position, in azimuth, of the receiver unit. The mounting of the receiver unit is so supported that it can be raised or lowered to adjust the elevation of the receiver unit. Moreover, a special rotational axis system holding the transducer at the bottom end of this frame, is designed to be rotated from the top in order to adjust its tilt angle in the vertical plane. A protractor is mounted on the top of this mechanism for a direct indication of this tilt. This complex setup enables one to adjust all the necessary parameters of the receiver transducer. The operator has a list of settings of range, tilt angle, altitude (depth here), and these are read on permanently mounted tape along the length of the tank protractor, and along the vertical leg of the special L-frame respectively. The accuracy of position is ± 1/32", and the tilt angle for the transducer is ± 0.1 degrees.

The 4' × 4' model runway is mounted, facing down into the water, on a specially designed frame, and coupled to a Scientific Atlanta positioning system mounted on top of the tank on a rigid platform supported by tank walls. The two scan units consist of plastic transducers in their respective holders, mounted in specially constructed frames so as to provide the azimuth and elevation scanning capability. This is achieved by connecting a flexible shaft from the positioning system shaft to the fixed shaft rotating transducer holder. Only one of the scan units was operated at any one time, whereas the other unit was removed in order to eliminate interference caused by the latter. The positioning accuracy of Scientific Atlanta system is ± 0.01 degrees.

The chase airplane models were hung by weight tied to a nylon fishing fiber below the model aircraft. Another tandem positioning connection was

provided outside the water in order to provide means to change their position relative to the shuttle receiver. These were manually positioned all over the space around the receiver, and were found to cause no multipath problems except when they were positioned in the common volume of the transmitter and the shuttle receiver. This occurred only when the chase planes were almost in-front (position) of the receiver.

The rain model discussed in Section 7 was installed at the bottom of the water tank, and compressed air at predetermined settings was passed through the air stones of the rain generating set in order to create a volume of random size bubbles simulating rain. Theoretical and practical justification for such a model is given in the next section.

The Scientific Atlanta positioning system is synchronized with the Scientific Atlanta Receive and Record System located at one end of the water tank by transmit and receive synchros. Thus the recording chart paper can be either manually or automatically controlled from the main controller. The scan speeds can be set by the setting of the chart speed controller, and the calibration of these speeds in degrees per second is given in Fig. 6.4. It was found necessary to operate at approximately 1.75 degrees per second in order to capture all the details and yet not be affected by the mechanical lag of the recording system.

The experimental data was taken by setting up the system for a given range, and the corresponding receiver tilt angle and elevation, under no rain conditions, and then repeating it under two rain settings R_1 and R_2 as shown in the rain runs for various ranges in the Appendix. A second receive transducer was located to the side of the one simulating the Orbiter receiver such a way as to be completely outside its main beam. This unit is called the

reference unit, and its position is kept fixed during the entire set of experimental runs. The reference transducer is electronically switched in after recording the major lobe as well as the following first null of the Orbiter receiver beam. The basic purpose of this receiver is to locate the position of -4 db beam center of the Orbiter receiver beam from a known and fixed reference point, thus enabling us to calculate the shift in the shuttle beam due to any multipath distortion may be called a location error for both azimuthal and elevation scan results. A typical calculation of the same is shown in Fig. 6.5.

A summary of all data analysis based on the above criterion is given in Table 6.1. An examination of the above data shows that ultrasonally simulated multipath errors in azimuthal and elevation shuttle scan beam locations are limited to a maximum of 0.08 degrees at 27,250 feet range for azimuthal scan and 0.125 degrees at 32,000 feet range for elevation scan.

A summary of errors analysis as obtained from simulation is given in Table 6.2. It is necessary to discuss some of the nomenclature used in reporting these results. The "NO-RUNWAY" condition implies that the receiver and transmitter are located at exactly the same relevant positions in free space as in the case of MSBLS in the presence of runway with its surrounding ground area. This data point is often used to determine the ground multipath as compared to the free space case. Furthermore the data is recorded in Tables 6.1, 6.2 and 6.3 in two basic formats:

Table 6.1 Actual -4 db beam points for both reference and MSBLS simulate receivers.

Table 6.2 Shift of -4 db beam center of the simulated MSBLS receiver with reference to that of the reference beam center (ΔR).

Table 6.3 Actual variation of the -4 db beam width of the simulated MSBLS receiver.

In view of the above, one has the option to examine the data from different viewpoint of the user.

TABLE 6.1 SUMMARY OF SIMULATED MSBLS DATA AND ANALYSIS

RUN #	TYPE	RECEIVER a_{-4}	RECEIVER a_{+4}	REFERENCE a_{-4}	REFERENCE a_{+4}	a_{Rx} $\frac{a_{-4}+a_{+4}}{2}$	a_{REF} $\frac{a_{-4}+a_{+4}}{2}$	DA
80209	DIST	AZ	SCANS	-NO RUNWAY -		NO	RAIN	
001	26.3"	13.5	23.5	154.5	166.5	18.5	160.5	142
002	35.3	10.5	19.5	155	167	15	161	146
003	51.8	8.5	18.5	160.5	169	13.5	164.75	151.25
004	68.8	0	12	150.5	161	6	155.75	149.75
005	85.7	14.5	28	169	177	21.25	173	151.75
006	102.2	-9	4	146.5	155	-2.5	150.75	153.25
007	120	-16	0	138.5	149	-8	143.75	151.75
80117		AZ	SCANS	-RUNWAY	-RAIN			
021	26.3" NR	4.5	16	147	160	10.25	153.5	143.25
022	35.3" NR	-7	4.5	142	153	-1.25	147.5	148.75
023	51.8 NR	7.5	19	158.5	171	13.25	164.75	151.5
024	68.8 NR	-3.5	7.5	149	162	2	155.5	153.5
	R_1	-3	7.5	149	162	2.25	155.5	153.25
	R_2	-3	7.5	149	162	2.25	155.5	153.25
025	85.7 NR	-1	10	152	162	4.5	157	152.5
	R_1	-1.5	10	151.5	161.5	4.25	156.5	152.25
	R_2	-1.5	10.5	152	162	4.5	157	152.5
026	102.2" NR	14	27.5	170	179	20.75	174.5	153.75
	R_1	13.5	26.5	168.5	179	20	173.75	153.75
	R_2	12.5	26.5	168.5	179	19.5	173.75	154.25
027	120 NR	19	34	173	182	26.5	177.5	151
	R_1	18	35	173	183	26.5	178	151.5
	R_2	-	-	173.5	184	-	178.75	-
801170			EL SCAN	RUNWAY -	RAIN			
028	35.3" NR	5.5	11.5	32.5	38	8.5	35.25	26.75
029	51.8" NR	0	5.5	55	61	2.75	58	55.25
030	68.8" NR	-4	1.5	60	65	-1.25	62.5	63.75
	R_1	-4.5	1.5	59	65	-1.5	62	63.5
	R_2	-4.5	1.5	59	65	-1.5	62	63.5
031	85.7 NR	-11	-4.5	57.5	63	-7.75	60.25	68
	R_1	-11	-4.5	57.5	63	-7.75	60.25	68
	R_2	-11	-4	57.5	63	-7.5	60.25	67.75
032	102.2 NR	-3.5	3.5	68	74	0	71	71
		-4	3	67.5	73	-0.5	70.25	70.75
		-4	3.5	67.5	73	-0.25	70.25	70.5
033	120" NR	8.5	15	82	87.5	11.75	84.75	73
	R_1	8.5	15	81	87	11.75	84	72.75

TABLE 6.2 SUMMARY OF SIMULATED MSBLS MULTIPATH

CAUSED -4 db BEAM (IN REFERENCE TO THE CORRESPONDING REFERENCE BEAM CENTER)

Actual Range (kilo ft)	Azimuth Scan			Elevation Scan		
	NR	R_1	R_2	NR	R_1	R_2
7.0	+0.209			Ref		
9.4	+0.455			Ref		
13.8	+0.043			Ref		
18.35	+0.625	-0.042	0.000	Ref	-0.042	-0.042
22.85	+0.125	-0.042	0.000	Ref	-0.000	-0.042
27.25	+0.083	0.00	0.083	Ref	-0.042	-0.083
32.0	-0.125	+0.081		Ref	-0.125	-0.125

NR = NO RAIN CONDITION

R_1 = RAIN RATE ONE

R_2 = RAIN RATE TWO

TABLE 6.3 SUMMARY OF SIMULATED MSBLS RECEIVER -4 db

BEAM WIDTH (x6)

Actual Range (kilo ft)	Azimuth Scan			Elevation Scan		
	NR	R_1	R_2	NR	R_1	R_2
7.0	12.5	*	*	**	*	*
9.4	11.5	*	*	6	*	*
13.8	11.5	*	*	5.5	*	*
18.35	11.0	10.5	10.5	5.5	6.0	6.0
22.85	11.0	11.5	12.0	6.5	6.5	7.0
27.25	13.5	13.0	14.0	7.0	7.0	7.5
32.0	15.0	17.0	***	6.5	6.5	7.0

* - Rain could not be simulated because of air bubble accumulation on model runway.

** - Physically not possible to run because of positional problem of equipment.

*** - Operational problems - data is questionable.

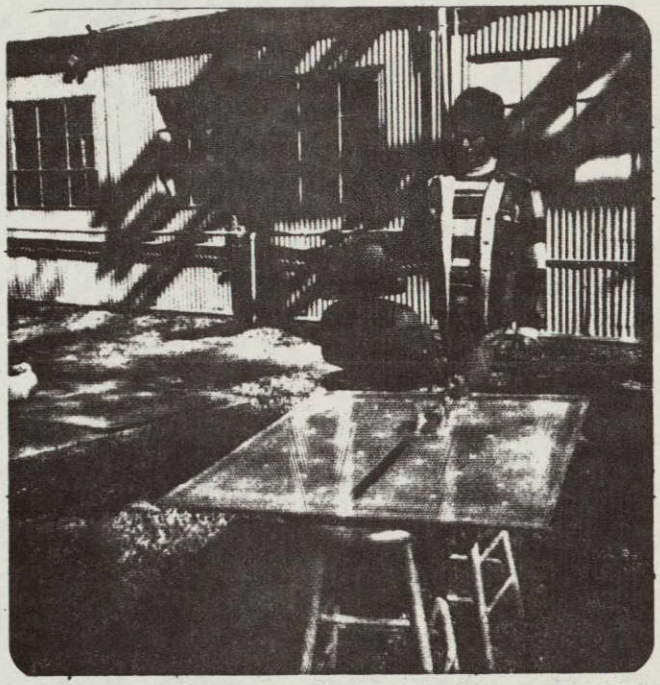

FIG. 6.1 ORBITER/747 - RUNWAY MODEL WITH AZIMUTH AND ELEVATION SCAN XDCR HOLDERS

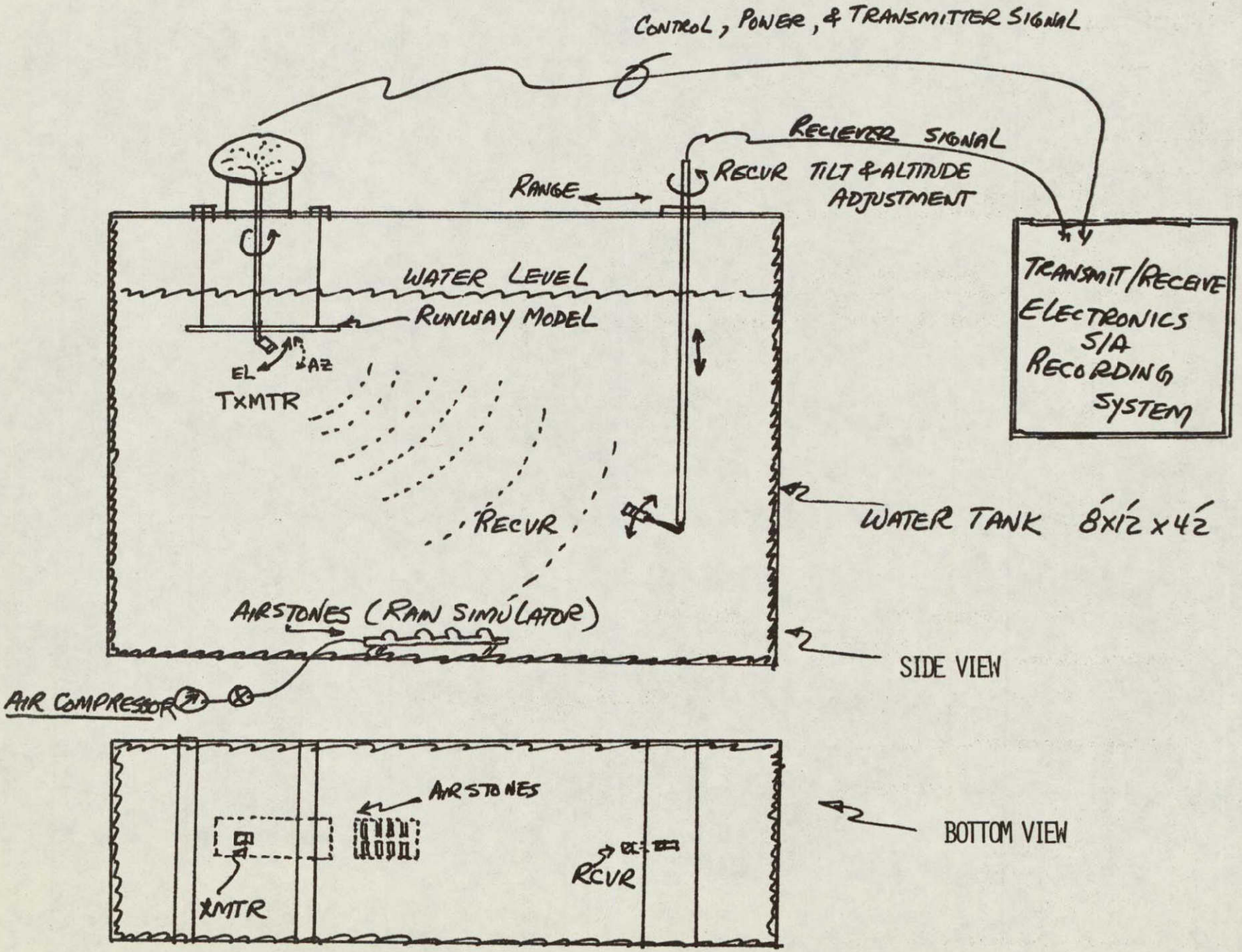

FIG. 6.1B SIDE & BOTTOM VIEWS - OVERALL SIMULATION SETUP

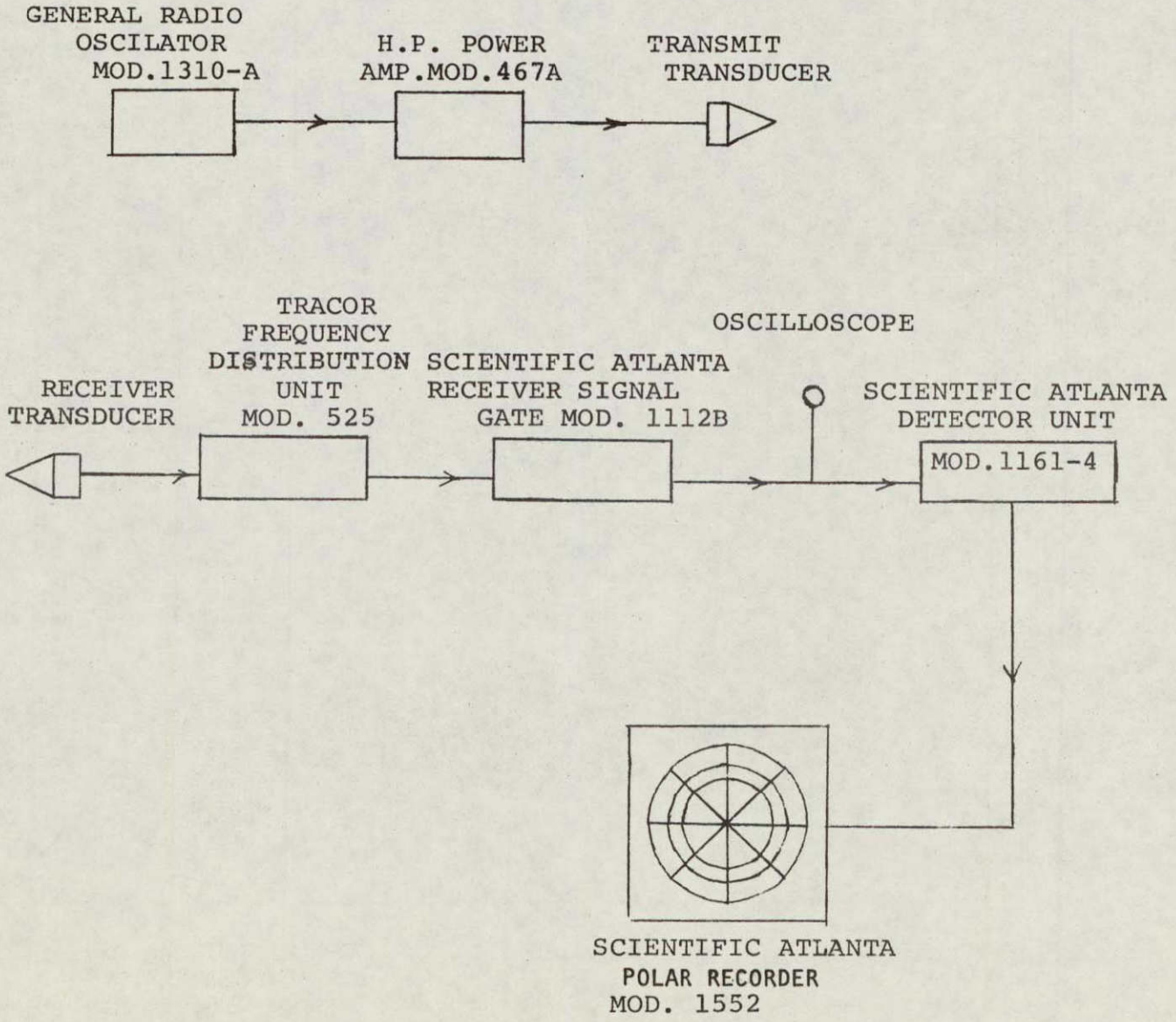

FIG. 6.2 ULTRASONIC SIMULATION SYSTEM BLOCK DIAGRAM

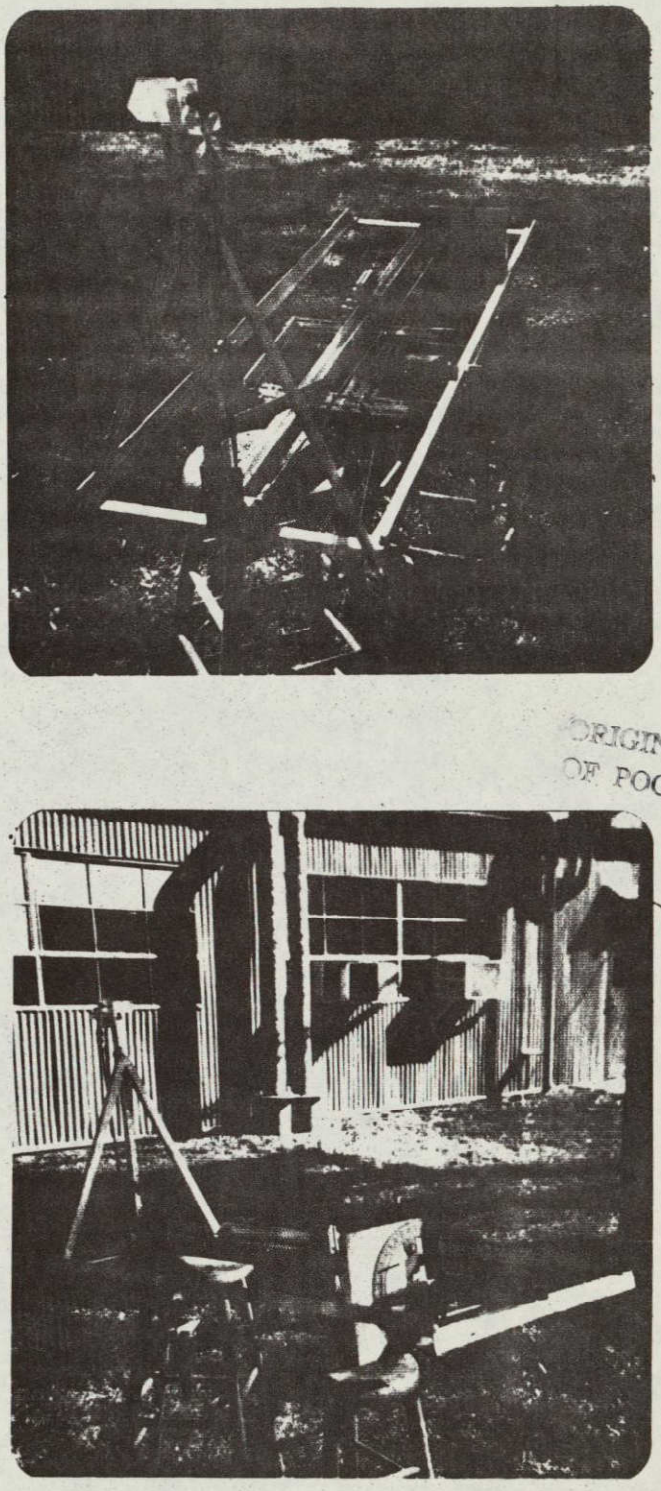

FIG. 6.3 ORBITER RECEIVER XDCR SUPPORT MECHANISM-TWO VIEWS

FIG. 6.4 SCAN SPEED CALIBRATION IN DEGREES PER SECOND SPEEDS ON SCIENTIFIC ATLANTA

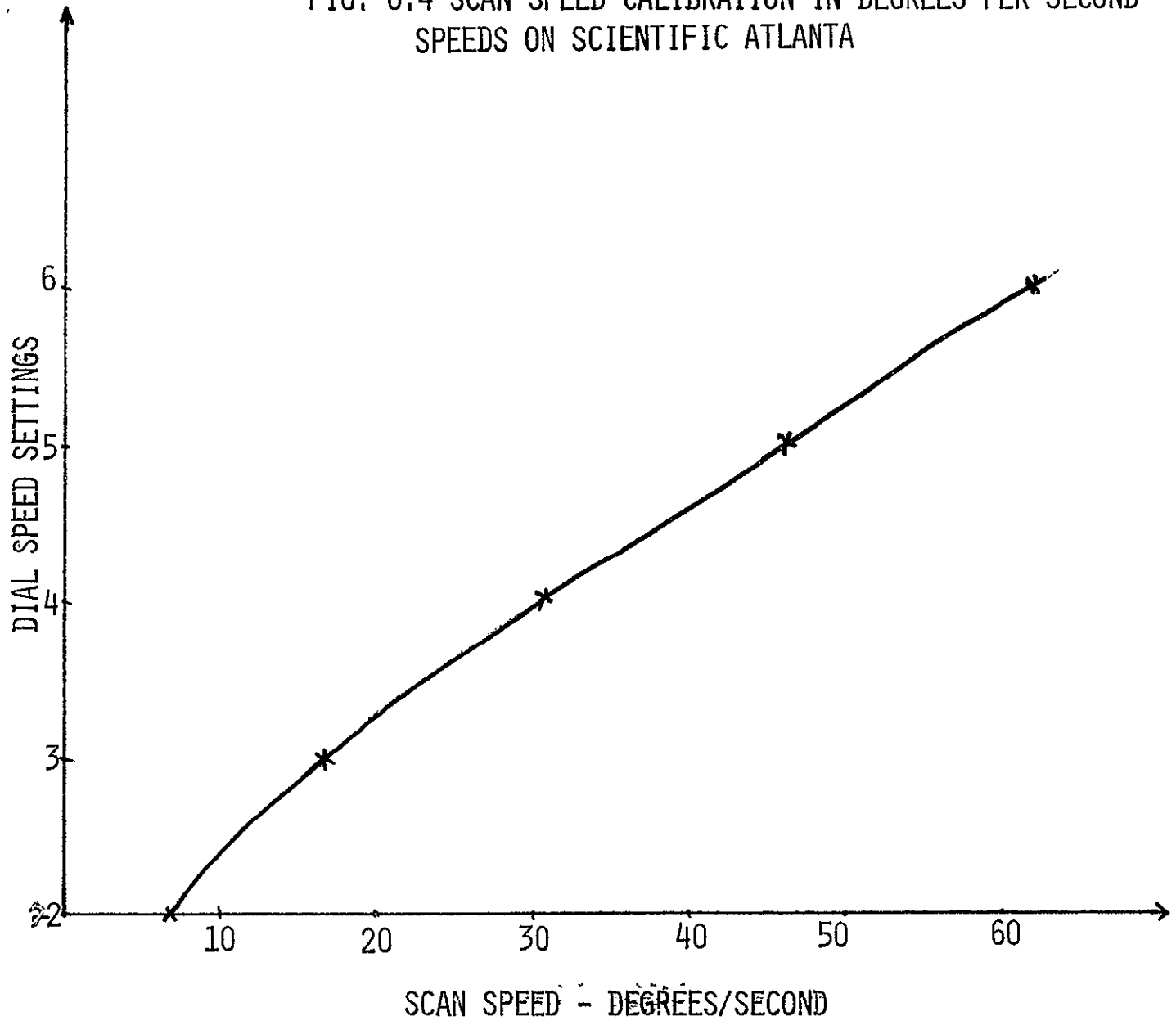

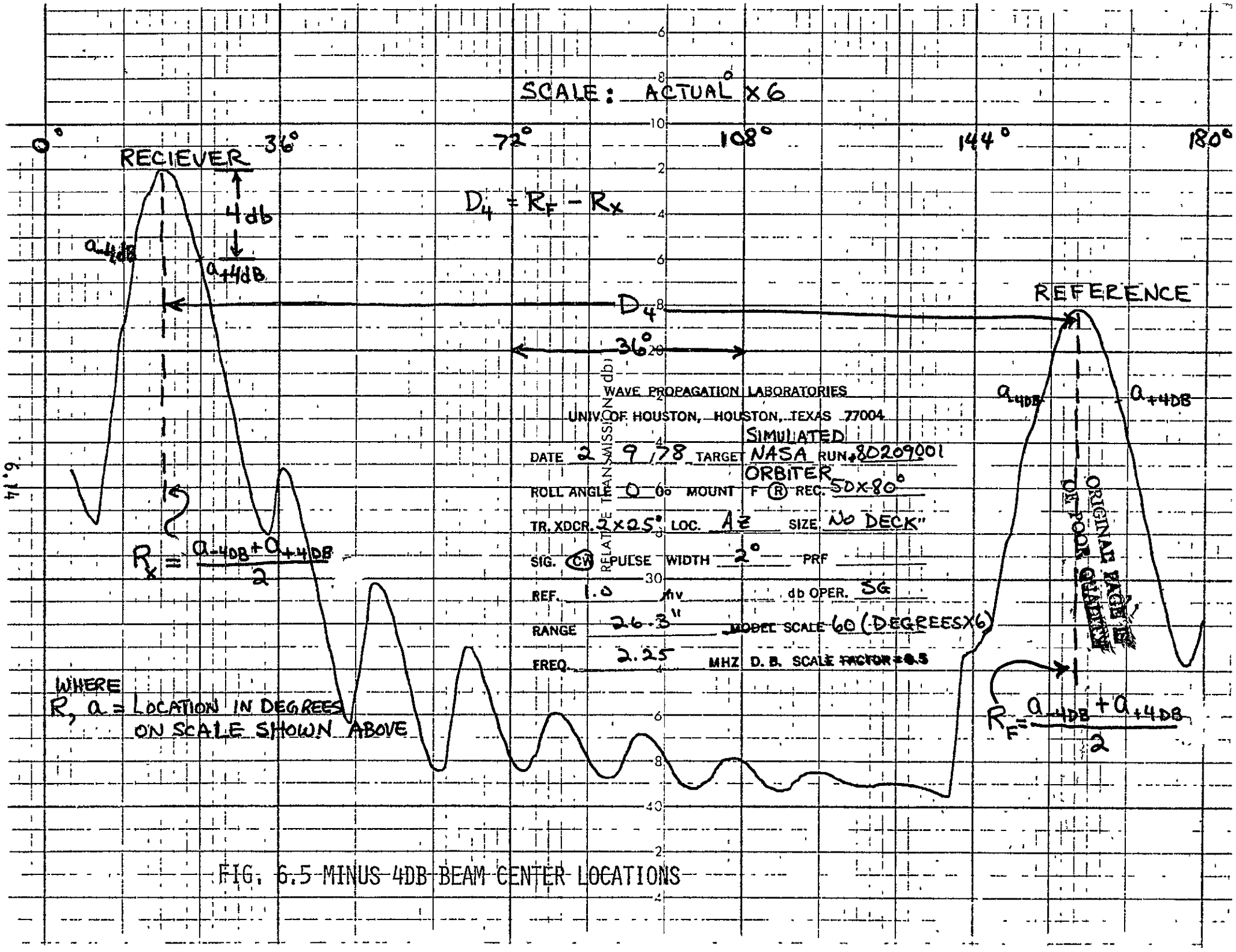

FIG. 6.5 MINUS 4DB BEAM CENTER LOCATIONS

7. ULTRASONIC SIMULATION OF RAIN

Multipath degradation of azimuth and elevation scan signals for ground-based transmitters and airborne receivers such as MSBLS are expected to get worse for light and heavy rainfall conditions as opposed to no-rain conditions. The main reasons for this effect are the different phase fluctuations of the direct, and indirect path signals because of

a) the intervening rain volume instead of free space,

b) the nonuniform rain distribution along both paths,

c) the propagation through rain volume at different angles (measured from the vertical) for both paths,

d) the additional random fluctuations of the amplitude and phase angle of the forward reflection coefficient from the ground points due to the time-varying ground surface disturbed by raindrops during rainfall,

e) the variation of the average attenuation and composite phase shift for a uniform rain volume path length.

It is often considered sufficient, in case of line-of-sight propagation paths, to assume the path attenuation, for uniform rain for a given propagation frequency to be:

$$\text{total db attenuation} = \text{No rain attenuation} + \text{rain caused attenuation}$$

$$= 20 \log (\lambda/4\pi r) + KR \qquad (7.1)$$

where K = constant db/n. miles, and it varies with rainfall rates and the operating frequency

R = range - n. miles

For instance, at a frequency of 15 gigahertz, one obtains the value of K as 1.67 db/nautical mile for 0.63 inches per hour of rainfall. This is quite satisfactory for line-of-sight communication paths where one is interested in long-time averaging of signals, but MSBLS requires accuracies of 0.05 degree, (equal to one standard deviation) and MSBLS updates its average positional readout averaging period approximately every 200 milli-seconds. It is quite obvious that long-time average attenuation or phase changes would not be very helpful in determining MSBLS multipath degradation in the presence of rain, let alone the multipath amplitude and phase effects of the rain effected ground as is the case for MSBLS.

It is also very pertinent to note that in all theoretical work in the area of rainfall attenuation and depolarization (Warner et al, 1976, Mink, 1976), rain drop shapes and their orientations models have been assumed for uniform rain drop size distribution and rain rate along the path. This assumption of uniform rain rate, and the use of average rain rate is questionable in the case of Kennedy Space Center environment which has experienced a very short duration squall of 11.52 inches/hour rain for 0.3 minutes (Gullick 1976). It is believed that during such extreme rainfall periods, one may encounter the worst case MSBLS multipath degradation. In order to predict the degradation, the rainfall is simulated by air bubble volume in water at room temperature, in which air bubble size and shapes are randomly distributed just as is the case with the rain drop sizes in the natural environment. First the theory of rain modeling is discussed and then are given experimental results of rainfall attenuation for different rain rates in order to have a base for comparison with full scale results. Furthermore,

the beam shape distortion caused by ground multipath for MSBLS, although smoothed out by faster scan rates, leaves an unsymmetrical beam which is considerably different for that obtained for the case of the line-of-sight propagation in rain volume.

RAIN DROP MODELING: AIR BUBBLE SIZE DETERMINATION

The modeling of rain drops is based on simulation of their radar cross-section and transmission coefficient of rain volume. The rain drops are simulated by air bubbles in a water tank, and acoustic sources with appropriate beamwidths are used to simulate electromagnetic sources of MSBLS. The air bubbles are formed by the flow of pressurized air through a set of fish stones located at the bottom of the tank. Let us first examine the details of the radar reflectivity of a static rain model.

The velocity of the falling speed of water for a rain drop of radius a cm is (Gunn and Kinzner, 1944)

$$V(a) = 950 \{1-\exp(-a/0.875)^{1.2}\} \text{ cm/sec} \tag{7.1}$$

Eq. (7.1) may be approximated by the following Eq. for the range $0.5 < a < 0.3$ cm.

$$V(a) = 950 \{1-\exp(-\mu a)\} \text{ cm/sec} \tag{7.2}$$

where $\mu = 11.2 \text{ cm}^{-1}$

The radar extinction cross-section of a single drop (Ryde and Ryde, 1944) can be approximated by

$$\sigma_{ext}(a) = 120a^{4.54} \text{ cm}^2 \tag{7.3}$$

and the extinction cross-section for the range .03 < a < .25 cm is given in Table 7.1 for λ = 3.2 cm.

The attenuation γ due to the rain drops is given below.

$$\gamma = \int_0^\infty N(a)\ \sigma_{ext}(a)\ da \tag{7.4}$$

where N(a) is the distribution function of the size of the rain drop and $\sigma_{ext}(a)$ is defined in Eq. (7.3). N(a) is assumed to follow the distribution function given by Khrgian and Mazin (1952) or

$$N(a) = Ca^2 e^{-\xi a} \qquad C = 54\ cm^{-6} \tag{7.5}$$

where ξ is a parameter (cm^{-1}) significant of the rain intensity, R, which is given as follows:

$$R = \int_0^\infty N(a)\ \frac{4\pi a^3}{3}\ V(a)\ da \tag{7.6}$$

Substituting V(a) and N(a) from Eqs. (7.2) and 7.5) in Eq. (7.6) one obtains:

$$R(\xi) = 7.75 \times 10^9 \left[\frac{5!}{\xi^6} - \frac{5!}{(\xi+\mu)^6}\right] \text{ mm/hr} \tag{7.7}$$

The values of R and γ for various values of ξ are given in Table 7.2 (Kwan, 1968) for λ = 3.2 cm.

The backscattered received power Pr is given by the following:

$$P_\gamma = P_t \frac{e^{-m\gamma c\tau}}{L_1} \frac{(L_2-L_1)}{L_2} \frac{G^2\lambda^2}{(4\pi)^3} \int_\theta\int_\phi f^4\ (\theta,\phi)d\phi\ d\theta \int_0^\infty$$

$$aN(a)\ da \tag{7.8}$$

where G = antenna gain

τ = the pulse length

m = an integer >> 1

(L_2-L_1) = thickness of the rain layer

λ = wavelength

P_t = transmitted power

C = velocity of light 3×10^8 m/sec

Φ,θ = antenna beamwidths

$f(\theta,\phi)$ = antenna beam

Substituting (Battaan, 1959) the value of G given below

$$G = \frac{\Phi\theta}{\int\int f^4(\theta,\phi)\,d\phi\,d\theta} \simeq 1.76$$

where

$$f^2(\theta,\phi) \simeq \exp - \left(\frac{\theta^2}{\Theta^2} + \frac{\phi^2}{\Phi^2}\right) 4 \text{ Ln } 2 \tag{7.9}$$

$$\int_0^\infty N(a)\, a\, da = \psi C \sum_{n=-\infty}^{\infty} \frac{W_n\, 81}{(\xi-inw)^9} \tag{7.10}$$

$$\psi = 4\pi\ (2\pi/\lambda)^4\ \left|\frac{\varepsilon_c-1}{\varepsilon_c+2}\right|^2 \tag{7.11}$$

W_n = the Fourier coefficients (Stephens, 1960) in

$$(\sigma_{MIE}/GRAY) = \sum_{n=-\infty}^{\infty} W_n\, e^{inw}$$

ε_c = complex permitivity of rain volume

in Eq. (7.8), one obtains:

$$P_r = \frac{P_t\lambda^2}{(4\pi)^3}\ \frac{1.76}{\Theta\Phi}\ \cdot\ \frac{e^{-m\gamma c\tau}}{L_1}\ \times\ \frac{L_2-L_1}{L_2}\ \psi\ C \sum_{n=-\infty}^{\infty} \frac{W_n\ 81}{(\xi-inw)^9} \tag{7.12}$$

The Mie Backscatter cross-section is given by:

$$\sigma_{mie} = \frac{\sigma_{mie}}{\sigma_{ray}} \cdot \sigma_{ray} = \psi\, a^6 \sum W_n\, e^{jnw} \tag{7.13}$$

where $\frac{\sigma_{mie}}{\sigma_{ray}}$ is tabulated by Stephen (1960), for a propagation wavelength of 3.2 cms. in Table 7.3, and one can write the following results:

$$\sigma_{ray} = 0.95 \times \frac{64\pi^5}{\lambda^4} a^6 = 1.83 \times 10^2 \; a^6 \tag{7.14}$$

for $\lambda = 3.2$ cm

The extinction cross-section of air bubbles for an acoustic source in water is (Urick, 1968) given below:

$$\sigma_e = \frac{4\pi\, a^2\, \delta/K_r a}{[(f_r/f)^2 - 1] + \delta^2} \tag{7.15}$$

where f_r = resonant frequency -Hz

δ = damping constant

a = radius of bubble -cm

$K_r = 2\pi f_\gamma / C_0$

C_0 = velocity of sound in water

The resonant frequency for a bubble is given as

$$f_r = \frac{326}{a} \; [1 + .03d]^{1/2} \tag{7.16}$$

where d the depth of the water in feet, and a is measured in centimeters.

For this rain simulation, d is assumed to be 3 feet and hence f_γ may be approximated by 326/a and $K_r a$ by .0186. In order to simulate the study of

radar cross-section due to rain drops, the size of air bubbles must be such that it gives the same scattering cross-section for the acoustic source. The radius of the air bubble a is given by the following equations:

$$a^6 + M_2 a^4 + M_1 a^2 + M_0 = 0 \tag{7.17}$$

where

$$M_2 = -\sigma_b (1 + \delta^2)/4\pi \tag{7.18}$$

$$M_1 = 2 \times (326)^2 \, \sigma_b / 4\pi f^2 \tag{7.19}$$

$$M_0 = -\sigma_e \, (326)^4 / 4\pi f^4 \tag{7.20}$$

The coefficients M_0 and M_2 are a less than unity at the frequencies of operation, viz, .01 mhz < f < 15 mhz, and therefore (7.16) becomes:

$$a^6 + M_2^2 a^4 = 0 \tag{7.21}$$

which has only real roots. An analytical solution of this Equation yields the bubbles radius given below:

$$a = \sqrt{\sigma_b / 4\pi} \qquad \text{for } a \sim \lambda \tag{7.22}$$

The size of the air bubbles for the frequency of 2.25 mhz are given in Table 7.4.

Furthermore one may use the coefficient of attenuation K_e in db/cm defined by the equation given below.

$$K_e = 4.34 \, \bar{n} \, \sigma_e \tag{7.23}$$

where

$\bar{n}$ = average number of bubbles per cm^3

σ_e = extinction cross-section of bubbles in cm^2

It is most pertinent to note, that one employs the probability distribution of diameter of bubbles in the case of underwater bubbles in the same manner as that for raindrops in the case of radar. The expression (7.23) may be modified to include the total volume of an V(a) contributed by bubbles in the beam in water, to obtain

$$K_e = 1.504 \times 10^3 \, v(a) \qquad (7.24)$$

This expression is analogous to total rain drop contributed volume of water in air for the case of radar.

CALIBRATION OF RAIN SIMULATOR

Since radio and radar frequency attenuation by rain volume has been usually reported in the literature in the form of average db/km attenuation. For instance Livingston (1970) reports an attenuation of 1.243 db/km for 15 mm/hour rain rate at 16 GHz, whereas Kerr (1951) summarizes rain attenuation measurements at the same frequency and for the same rain rate to be 1.65 db/cm. Furthermore McCormick et al. (1976) report that attenuation rates of 1 to 15 db/km at 16.5 GHz measured over a long period of observation varying from 1972-1975, and further show the importance of canting angle. The basic reasons for such a broad range of variations are:

1) the rain volume attenuation measurements are averaged over many minutes and in fact up to an hour or so at many times

2) the rain volume is assumed to have a uniform rain rate

3) the extent of rain free air volume in the radar path is not known to the experimenters

4) there is no ground multipath, as in the case of MSBLS, which could further broaden the range of attenuation.

In view of the above, it was decided to use an average attenuation figure from Livingston (1970) for 15GHz frequency, to calibrate the rain simulator. Airstones spanning a simulated range of 28 inches (corresponding to a full scale MSBLS range of 2.28 kilometers) were used to generate continuous rain volume and the transmitter/receiver were set up in their usual location in the MSBLS geometry so that the rain caused fading statistics would be more meaningful than that affecting a radar beam traversing a rain volume at right angle to the path of the rain drops. The theoretically verified experimental rain attenuation data at 15 GHz used in this calibration is given below:

Rain Rate mm/hr (IN/HR)	Attenuation db/Km
4.0 (0.16)	0.30
10.0 (0.39)	1.15
20 (0.79)	2.4
30 (1.18)	3.6
40 (1.57)	4.5
50 (1.97)	5.3

Based on the above reference data, the simulated rain rates R_1 and R_2 were found to be equivalent to 0.31"(7.8 mm/hr) and 0.61" (11.5 mm/hr) inches per hour respectively, since attenuation caused by rain only of 2 and 4 db were found to occur for a simulated 28" (equivalent to 2.276 Km full scale) long rain volume along the path of the simulated radar beam. The canting angle of the simulated radar beam was taken into account in calculating the

equivalent rain rates.

FADING DEPTH

The multipath caused fading depths are measured in db excursions from the average signal level. Both experimental and theoretical rain caused fading data for 15 GHz signals (Goldhirsh 1975) show that, for a thunderstorm or cloudburst (approximately 100 mm/hr or 3.94"/hr rain rate), the probability P(d>D) of the fade depths exceeding a given fade depth D for MSBLS radar beam tilts may be as given below; along with projected values for 1"/HR rain:

P(d>D) - Percent Time	Fade Depths - D db	
	100 mm/HR	25.4 mm/HR
20.0	2.56	0.56
15.0	5.12	2.58
6.0	10.24	5.18
3.5	15.39	10.3
2.5	20.48	15.4
1.8	25.6	20.5
1.5	30.78	25.7

The fade depths for simulated rain rates of R_1 and R_2 were found to be 3.13 and 7.88 db respectively, which were exceeded approximately 6 and 3 percent of the time. These fading statistics fall within the expected ranges calculated from data and discussion by Goldhirsh (1975) and Crane (1975).

MSBLS RAIN MULTIPATH SIMULATED RESULTS

Two simulated uniform rain rates R_1 and R_2, described above, were used to collect data on MSBLS receiver beam shape in order to study the multipath effect on its -4 db width. Only 28" (2.276 K m in full scale case) of the

total horizontal path length contained rain, and this extent of simulated rain volume was approximately 23% of the maximum simulated horizontal range (120").

In the case of MSBLS ultrasonic simulation, the radar signal back-and forward-scattered by rain volume is appropriately reproduced in simulated rain in the form of air bubbles in water. For instance, MSBLS guidance signal at approximately 15.55 GHz (1.93 cm, wavelength) is simulated by 2.25 mhz (0,667 mm wavelength) ultrasonic azimuth and elevation scan signals with appropriate waveform and beamwidths. The time varying wind as well as rain intensity achieved by controlling the compressed air flow used for generating bubbles and simulating wind gusts by a jet of water blown into this volume of air bubbles were not incorporated because of severe fading obtained without these.

The minus four db receiver beamwidths for the simulated MSBLS case are listed in Table 7.5. The effect of the presence of rain apparently is to widen the said beamwidth in general by up to 2 degrees, whereas in few cases a reduction of up to 0.5 degree takes place. This is significant since these changes correspond to up to +13.3% increase&of -4.5% decrease respectively of the no rain condition case values. In the case of one inch rate, one would expect these changes in minus 4 db beamwidths to be more pronounced and of the order of up to +23% and probably no reductions. The ultrasonic simulation provided very extensive fading data discussed above.

TABLE 7.1 BUBBLE SIZE AND ITS EXTINCTION CROSS SECTION

Bubble / Drop Size (cm)	$\text{Log}_{10} e^{\sigma_{ext}(a)}$ cm^2
.03	6.5×10^{-6}
.04	2.5×10^{-5}
.05	7×10^{-5}
.06	1.5×10^{-4}
.08	5×10^{-4}
.10	1.5×10^{-3}
.15	9×10^{-3}
.20	3×10^{-2}
.25	8×10^{-2}

TABLE 7.2 RAIN INTENSITY (R) AND ATTENUATION (db/m)

R mm/hr-	ξ	(m^{-1})	$10 \text{ Log}_{10} e^{-\gamma}$ db/meter
170	40	1.1×10^{-3}	4.75×10^{-3}
100	43.7	$.56 \times 10^{-3}$	2.43×10^{-3}
43	50	$.2025 \times 10^{-3}$	0.88×10^{-3}
13	60	$.51 \times 10^{-4}$	2.21×10^{-4}
4.66	70	$.16 \times 10^{-4}$	$.694 \times 10^{-4}$
1.93	80	$.58 \times 10^{-5}$	2.51×10^{-5}
0.88	90	$.236 \times 10^{-5}$	1.02×10^{-5}

TABLE 7.3 RAIN-DROP BACKSCATTERING CROSS SECTION

a-cm	$\sigma_{mie}/\sigma_{ray}$	σ_{ray}	σ_{MIE} (Backscattered Cross Section)
.05	1	2.75×10^{-6}	$.275 \times 10^{-5}$
.075	0.9	$.32 \times 10^{-4}$	$.28 \times 10^{-4}$
.1	0.85	$.183 \times 10^{-3}$	$.16 \times 10^{-3}$
.125	0.75	$.7 \times 10^{-3}$	$.53 \times 10^{-3}$
.15	0.80	$.21 \times 10^{-2}$	$.17 \times 10^{-2}$
.175	1.35	$.53 \times 10^{-2}$	$.72 \times 10^{-2}$
.2	2.35	$.116 \times 10^{-1}$	$.27 \times 10^{-1}$
.225	2.4	$.24 \times 10^{-1}$	.0576
.25	2.4	$.44 \times 10^{-1}$	.105
.30	1.8	$.96 \times 10^{-1}$	.173
.35	1.65	.335	.552
.40	1.4	.74	1.04
.45	1.1	1.484	1.63
.50	1	2.97	2.97

TABLE 7.4 AIR BUBBLE RADIUS FOR DIFFERENT BACKSCATTERED CROSS-SECTIONS AT 2.25 MHZ

Desired Backscattered Crosssection	Bubble Size - mm
12.57	1
50.28	2
113.13	3
201.12	4
314.25	5
452.52	6
615.93	7
804.48	8
1018.17	9
1257	10
2828	15
5028	20

TABLE 7.5 MINUS FOUR DB RECEIVER BEAMWIDTH (DEGREES) OF ULTRASONICALLY SIMULATED MSBLS

Simulated Range (in) Conditions	26.3	35.3	51.8	68.8	85.7	102.2	120
AZ - No Rain	11.5	11.5	11.5	11.0	11.0	13.5	15.0
AZ - Rain R_1	----	----	----	10.5	11.5	13.0	17.0
AZ - Rain R_2	----	----	----	10.5	12.0	14.0	----
AZ - Rain R_3	12.0	12.2	12.5	13.0	13.5	15.0	18.5
EL - No Rain	6.0	5.5	5.5	5.5	6.5	7.0	6.5
EL - Rain R_1	----	----	----	6.0	6.5	7.0	6.5
EL - Rain R_2	----	----	----	6.0	7.0	7.5	7.0
EL - Rain R_3	6.1	6.0	6.3	6.5	7.5	8.0	7.5

Notation

R_1 = 0.31"/HR (7.8 mm/HR), R_2 = 0.61"/HR (11.5 mm/HR)

R_3 = 1"/HR (25.4 mm/HR) Projected values of beamwidth changes.

-- = No rain data available because of accumulation of air bubbles on simulated runway surface.

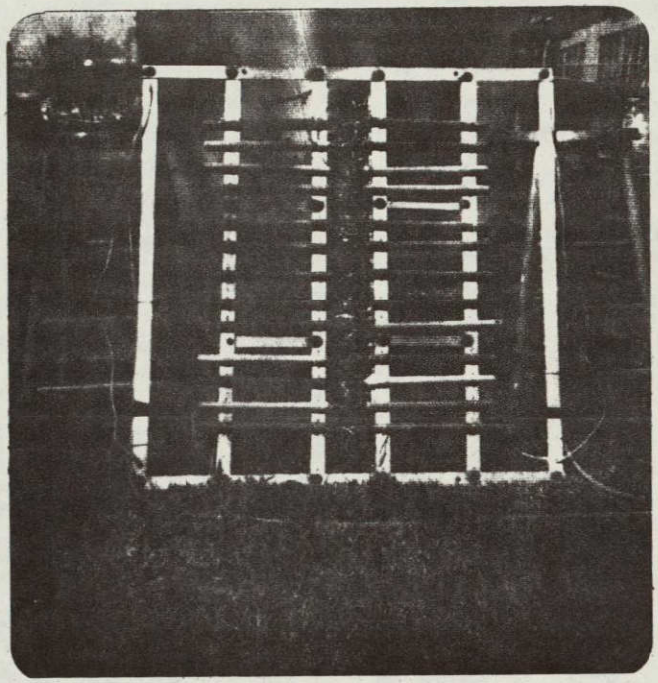

FIG. 7.1 RAIN GENERATION AIR STONES SETUP

8. Conclusions

MSBLS antenna coverage, landing trajectory and the ground plan containing the runway and its surrounding area were ultrasonically simulated. Fixed points were selected on the trajectory for collecting MSBLS simulated fading data for no rain, and two rain rate conditions of 0.31" and 0.61" per hour. Rain was simulated by air bubbles of random radii generated by air stones in water.

Rain caused minus 4 db beamwidth fading for 0.31"/HR simulated rain (R_1) was found to vary from -4.5 to 13.3%, and 0 to 9.1% for Az and El - beams respectively. The corresponding range from -4.5 to 16.7%, and 7.1 to 9.1% respectively were obtained for 0.61"/HR rain (R_2). Similar projected values for 1.0"/HR (R_3) were found to be 4.4 to 23.3% and 1.7 to 14.2% for AZ and EL beams respectively.

The fade depths with a probability of occurrence of 15% for R_1, R_2 and R_3 rain rates were obtained as 0.5, 0.9 and 2.56 db respectively, whereas those for 6% occurrence these values become 3.6, 4.5, and 5.18 respectively. It is noteworthy to add that fade depths of 24.1, 25, and 25.7 db may occur 1.5% of the time for R_1, R_2 and R_3 respectively.

Cloudburst, common to Cape Kennedy, defined as 100 mm/HR (3.94"/HR) may cause a fade depth of 2.56 db twenty percent of the time and 5.12 db fifteen percent of the time. The corresponding minus 4 db receiver beamwidths are expected to fluctuate far more severely for this case, such as 30-50% of the rain beamwidth values.

The fade depths as well as fluctuation of the simulated minus 4 db receiver beamwidth don't seem to follow a systematic range variation because of the nonlinear relationship of the illuminated ground area. Another sig-

nificant result of this simulation is that the simulated receiver beam shape is considerably more distorted by rain than indicated by the minus 4 db beamwidth variation. This will effect the MSBLS receiver output subject to the analysis process, and its sensitivity, since a jagged beam will display sudden changes in slope from one sample pulse to the next, and the orbiter system may just keep dropping off such sample values and if such severe environmental conditions continued to recur in a complete cycle, the whole cycle may result in a complete blanking of the guidance data for the said cycle. Of course, if the MSBLS receiver smooths out the input data, then it may overcome such major fluctuations in the signal amplitude caused by degradation of the receiver beam shape.

The actual percent path length containing no rain can make a considerable difference in the validity of the standard rain attenuation formula and associated average rain attenuation rates. In real time fast systems such as MSBLS, there is considerable fluctuation of the signal, and it is anticipated that MSBLS sampled data points taken on a beam would experience all the random fluctuation of the rain attenuation as well as those caused by the phase and amplitude fluctuations caused by ground multipath as opposed to that experienced by a direct path.

The effect of chase aircraft as a multipath degradation defect was found to be negligible, in fact the recorder could not record any noticeable difference in the beamshape as compared to the case without chase aircraft due to the narrowness of the azimuth elevation fan beams.

Finally the results obtained in the ultrasonic simulation at the University of Houston - Wave Propagation Lab are believed to a reasonably prediction of the full scale results.

It is recommended that a detailed crosscorrelation field data, and UH simulated data should be performed.

9. REFERENCES

1. Hayre, H. S., "Ultrasonic Fading Simulation", IEEE Trans-Sonics and Ultrasonics, Vol. SU 20, No. 1, January 1973, pages 32-33.

2. Hayre, H. S., "Ultrasonic Simulation of Radar Problems: Theory and Practice, University of Houston-Wave Propagation Laboratory - EE Department TR 73-11 (Revised 1974).

3. Stratton, A. J., "Electromagnetic Theory", McGraw Hill Book Co., New York, N. Y., 1941.

4. Hayre, H. S., "A-7 I.L.S. Antenna Coverage and Simulation", 1976 - URSI - AP - IEEE SYMPOSIUM, University of Massachusetts, October 1976 Digest, pages 1-4.

5. Hayre, H. S., M. Williamson, "Ultrasonic Modeling of a Naval Carrier Microwave Landing System", Proceedings Southwest IEEE Conference, University of Texas, Austin, Texas, IEEE Publication, pages 1-6, April, 1976.

6. Brekhovskikh, L. M., "Waves in Layered Media", Academic Press, New York, N. Y., 1960.

7. Hayre, H. S., "Acoustic Simulation of Moon Echoes", Abstract, Proc. URSI - IRE, Fall 1961 Conf., Oct. 1961, pages 22-23.

8. Hayre, H. S., "Ultrasonic Simulation of Target Characteristics and the Environment/Atmosphere", Proc. NATO Adv. Study Inst., 1975, Goslar, W. Germany.

9. Morse, Phillip M., Ingard, Uno K., Theoretical Acoustics, McGraw Hill, 1962.

10. Hayre, H. S., "Ultrasonic Simulation of MLA Aircraft Carrier Multipath" - Final Report on U. S. Navy Contract #N00421-75-R-0267, University of Houston, W. P. Lab-E.E. Dept., Houston, Texas, 77004 - January 20, 1978.

11. Gulick, J. R., "Percentage Frequency of Observed Maximum Rainfall Rates at Kennedy Space Center" - personal communication 1976.

12. Kwan, Stephen C. "Radar Reflectivity Study of Static Rain Model," M.S. Thesis-E.E. Dept., University of Houston, Houston, Texas, 77004 (under the direction of Dr. H. S. Hayre), 1968.

13. Gunn, K. L. S. and G. D. Kinzer, "The Terminal Velocity of Fall for Water Droplets in Stagnant Air," J. of Meteor., Vol. 6. 1949, pp. 243-248.

14. Ryde, J. W. and D. Ryde, Attenuation of Centimeter Waves by Rain, Hail, and Clouds, General Electric Company Research Labs., Wembley, England, Rept. No. 8516, August, 1944.

15. Khrgian, A. Kh. and I. P. Mazin, "Distribution of Drops According to Size in Clouds," Tr. Central Aerolog. Obs. (USSR), No. 7, 1952, pg. 56.

16. Battan, L. J., Radar Meteorology, University of Chicago Press, 1959.

17. Stephens, J. J., "Radar Cross-Sections for Water and Ice Spheres," J. of Meteor., Vol. 18, 1960, pp. 348-350.

18. Hayre, H. S. and R. K. Moore, Radar Back-Scatter Theories for Near-Vertical Incidence and Their Application to an Estimate of the Lunar Surface Roughness, Engineering Experiment Station, University of New Mexico, Report. No. EE-67, January, 1962.

19. Livingston, D. C., "The Physics of Microwave Propagation," Prentice-Hall, Inc., Englewood Cliffs, N. J., 1970.

20. McCormich, G. C. et al., "Depolarization Over a Link Due to Rain: Measurement of the Parameters," Radio Science Vol. II, No. 8, 9, pp. 741-749, August-September 1976.

21. Goldhirsh, J. "Prediction Methods for Rain Attenuation Statistics at Variable Path Angles and Carrier Frequencies Betweeen 13 and 100 GHz," IEEE Trans. Ant. & Prop., Vol. AP 23, No. 6, November 1975, pp. 786-791.

22. Kerr, A. D. (Editor), "Propagation of Short Radio Wave," M.I.T. Radiation Lab. Series, McGraw-Hill Book Co., New York, 1951.

10. APPENDIX

LIST OF RUNS AND RUN DESCRIPTION

RUN NO. AZ/EL	RANGE (k·ft.)	RAIN (R_1, R_2) NO RAIN (NR)	FREESPACE (FS) RUNWAY (RW)
80209001-AZ	7.0	NR	FS
9002-AZ	9.4	NR	FS
9003-AZ	13.8	NR	FS
9004-AZ	18.35	NR	FS
9005-AZ	22.85	NR	FS
9006-AZ	27.25	NR	FS
9007-AZ	32.00	NR	FS
80117021-AZ	7.00	NR	RW
7022-AZ	9.4	NR	RW
7023-AZ	13.8	NR	RW
7024-AZ	18.35	NR, R_1, R_2	RW
7025-AZ	22.85	NR, R_1, R_2	RW
7026-AZ	27.25	NR, R_1, R_2	RW
7027-AZ	32.00	NR, R_1, R_2	RW
7028-EL	9.4	NR	RW
7029-EL	13.8	NR	RW
7030-EL	18.35	NR, R_1, R_2	RW
7031-EL	22.85	NR, R_1, R_2	RW
7032-EL	27.25	NR, R_1, R_2	RW
7033-EL	32.00	NR, R_1, R_2	RW

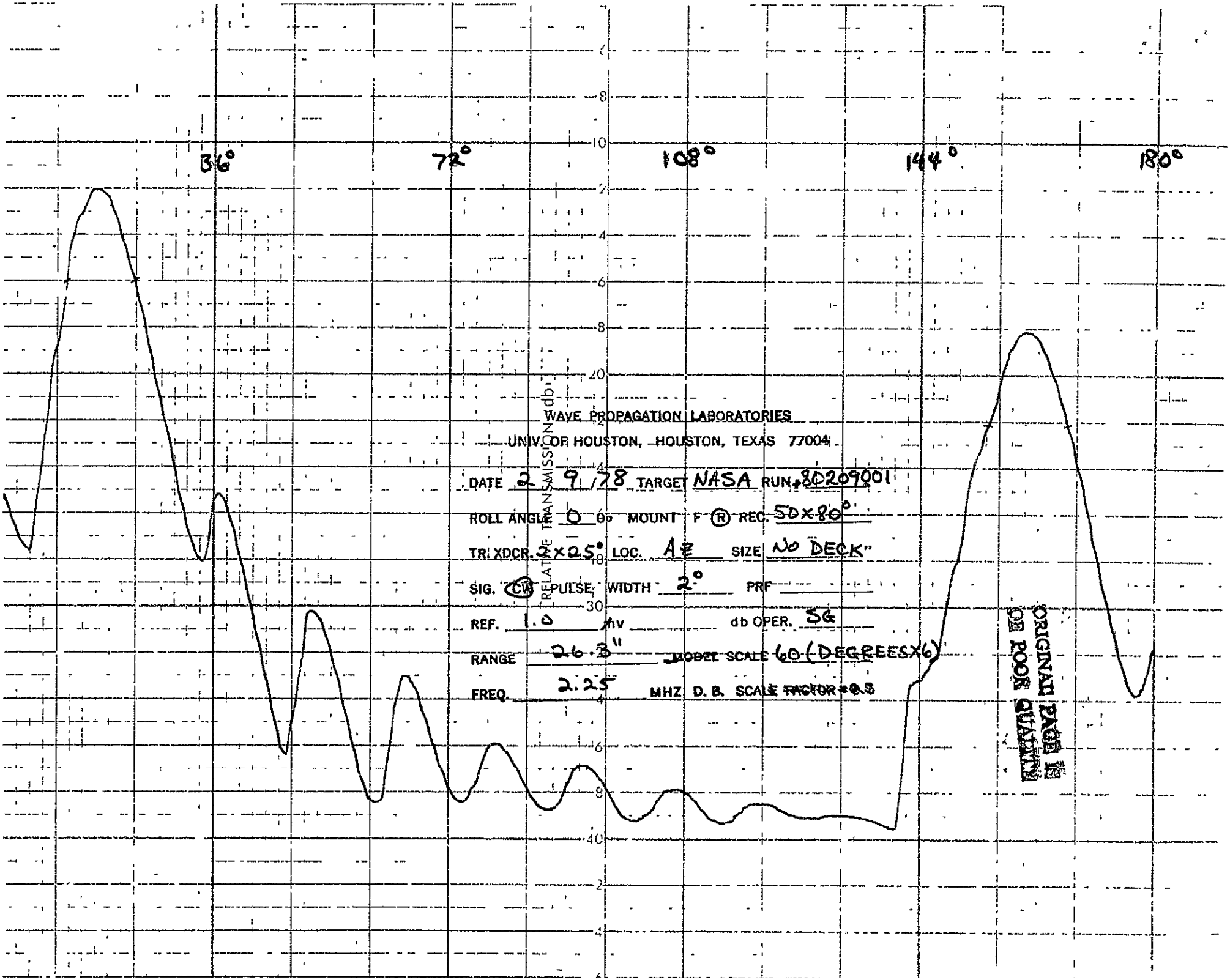

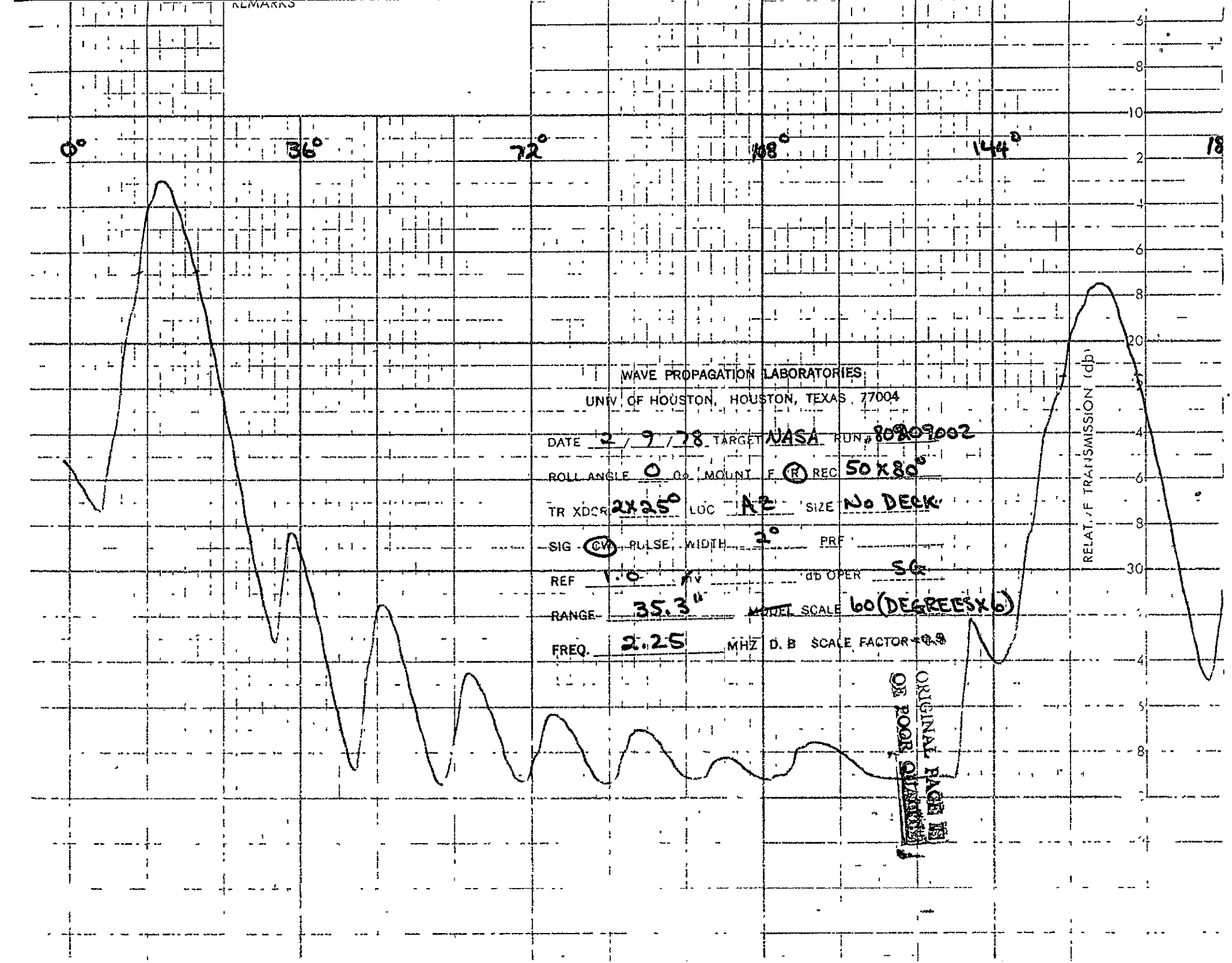
REMARKS
0°
36°
72°
108°
144°
18
WAVE PROPAGATION LABORATORIES
UNIV. OF HOUSTON, HOUSTON, TEXAS 77004
DATE 2/9/78 TARGET NASA RUN # 80209002
ROLL ANGLE 0 0° MOUNT F (R) REC 50 X 80°
TR XDCR 2X25° LOC A2 SIZE No DECK
SIG (CW) PULSE WIDTH 3° PRF
REF 1.0 dv db OPER 56
RANGE 35.3" MODEL SCALE 60 (DEGREES X 6)
FREQ. 2.25 MHZ D. B SCALE FACTOR +0.9
RELATIVE TRANSMISSION (db)
ORIGINAL PAGE IS OF POOR QUALITY

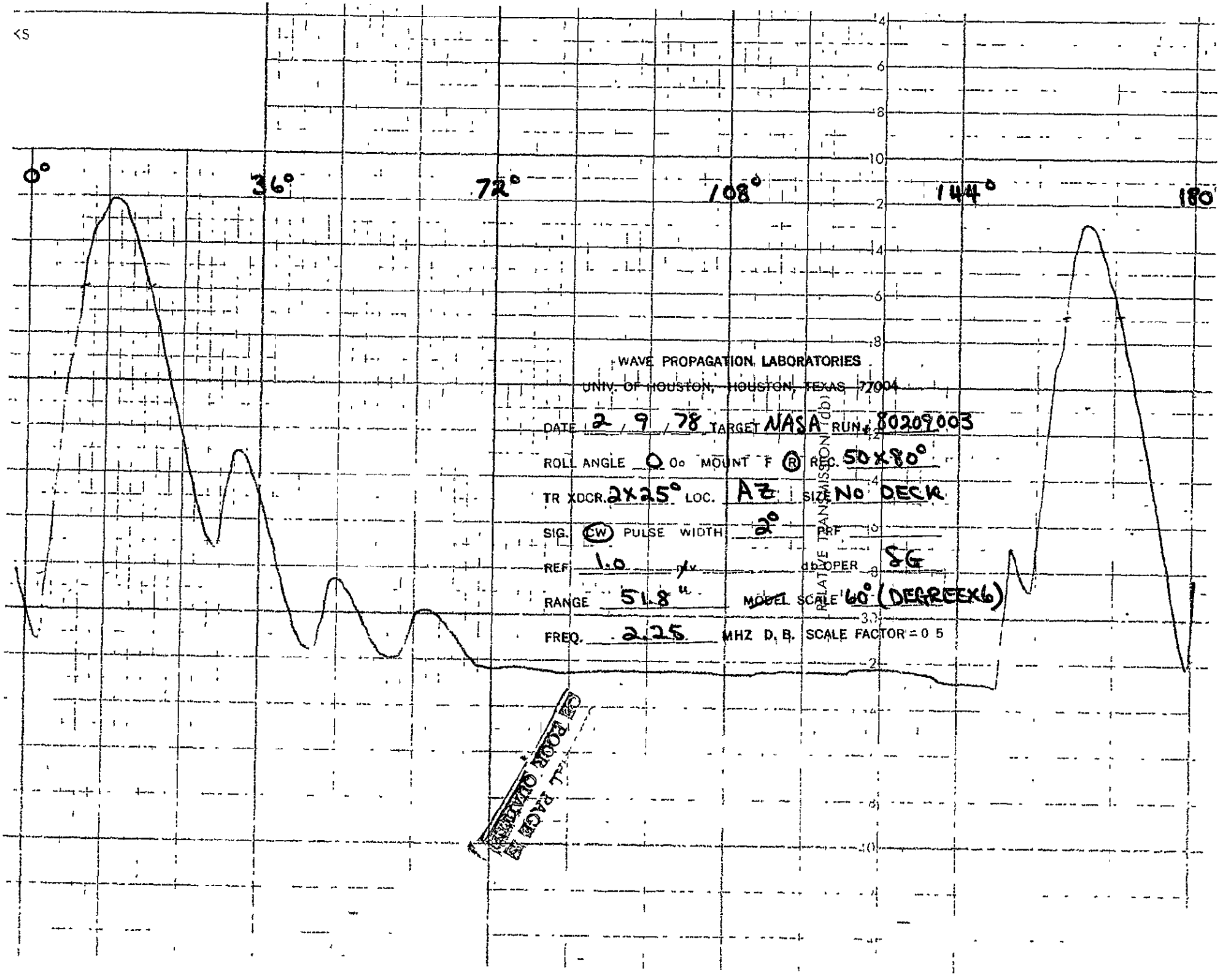
0°
36°
72°
108°
144°
180
WAVE PROPAGATION LABORATORIES
UNIV. OF HOUSTON, HOUSTON, TEXAS 77004
DATE 2 / 9 / 78 TARGET NASA RUN # 80209003
ROLL ANGLE 0.0o MOUNT F (R) REC. 50x80°
TR XDCR. 2x25° LOC. AZ SIZE No DECK
SIG. (CW) PULSE WIDTH 2° PRF
REF 1.0 mv db OPER SG
RANGE 51.8 u MODEL SCALE 60° (DEGREEX6)
FREQ. 2.25 MHZ D.B. SCALE FACTOR = 0 5
RELATIVE TRANSMISSION (db)
BEST AVAILABLE COPY
FOLD OUT PAGE

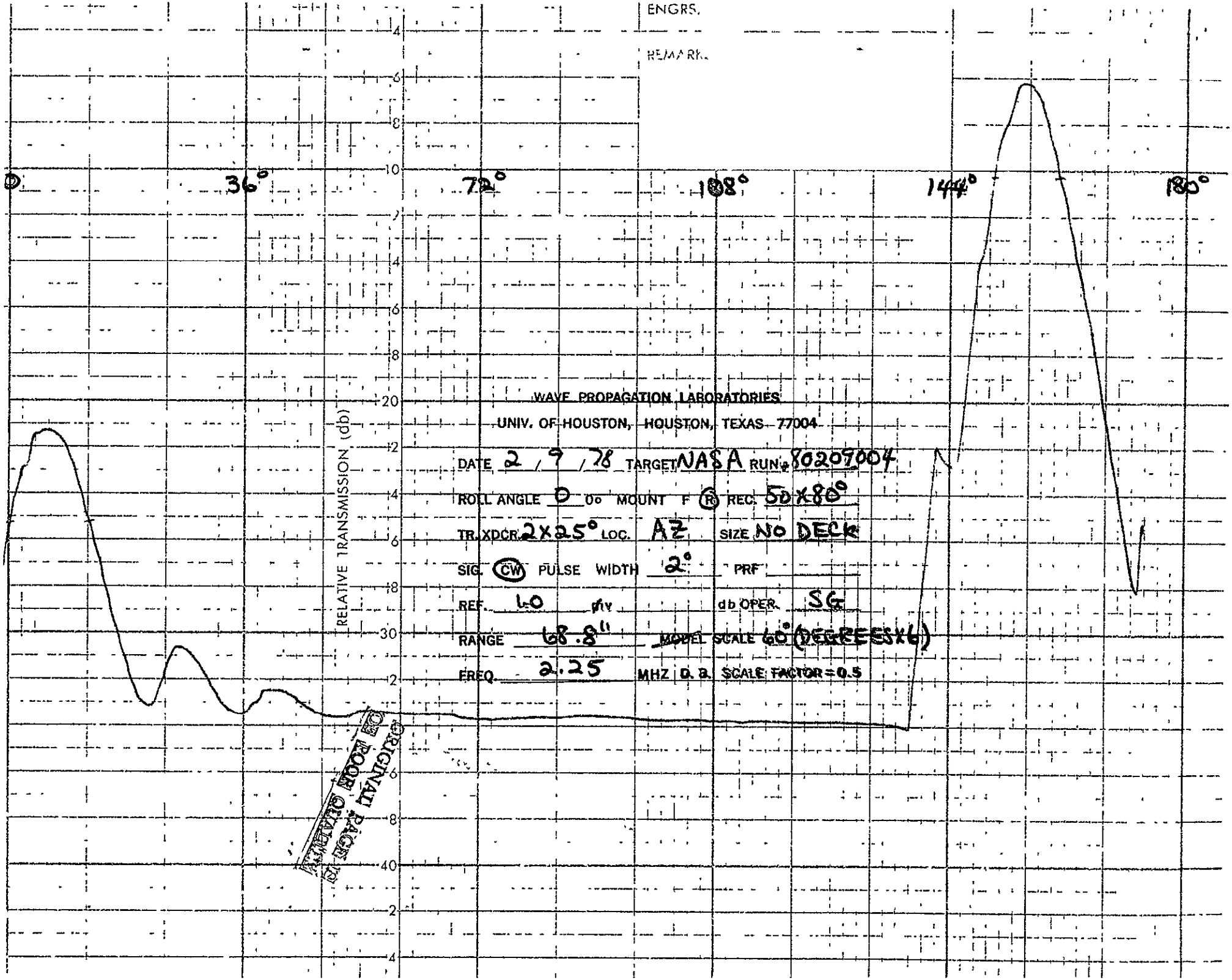
ENGRS.
REMARKS
0°
36°
72°
108°
144°
180°
RELATIVE TRANSMISSION (db)
WAVE PROPAGATION LABORATORIES
UNIV. OF HOUSTON, HOUSTON, TEXAS 77004
DATE 2 / 9 / 78 TARGET NASA RUN # 80209004
ROLL ANGLE 0 0° MOUNT F (R) REC. 5D X 80°
TR. XDCR. 2X25° LOC. AZ SIZE NO DECK
SIG. (CW) PULSE WIDTH 2° PRF
REF. 6.0 div db OPER. SG
RANGE 68.8' MODEL SCALE 60° (DEGREES X 6)
FREQ. 2.25 MHZ D. B. SCALE FACTOR = 0.5
ORIGINAL PAGE IS OF POOR QUALITY

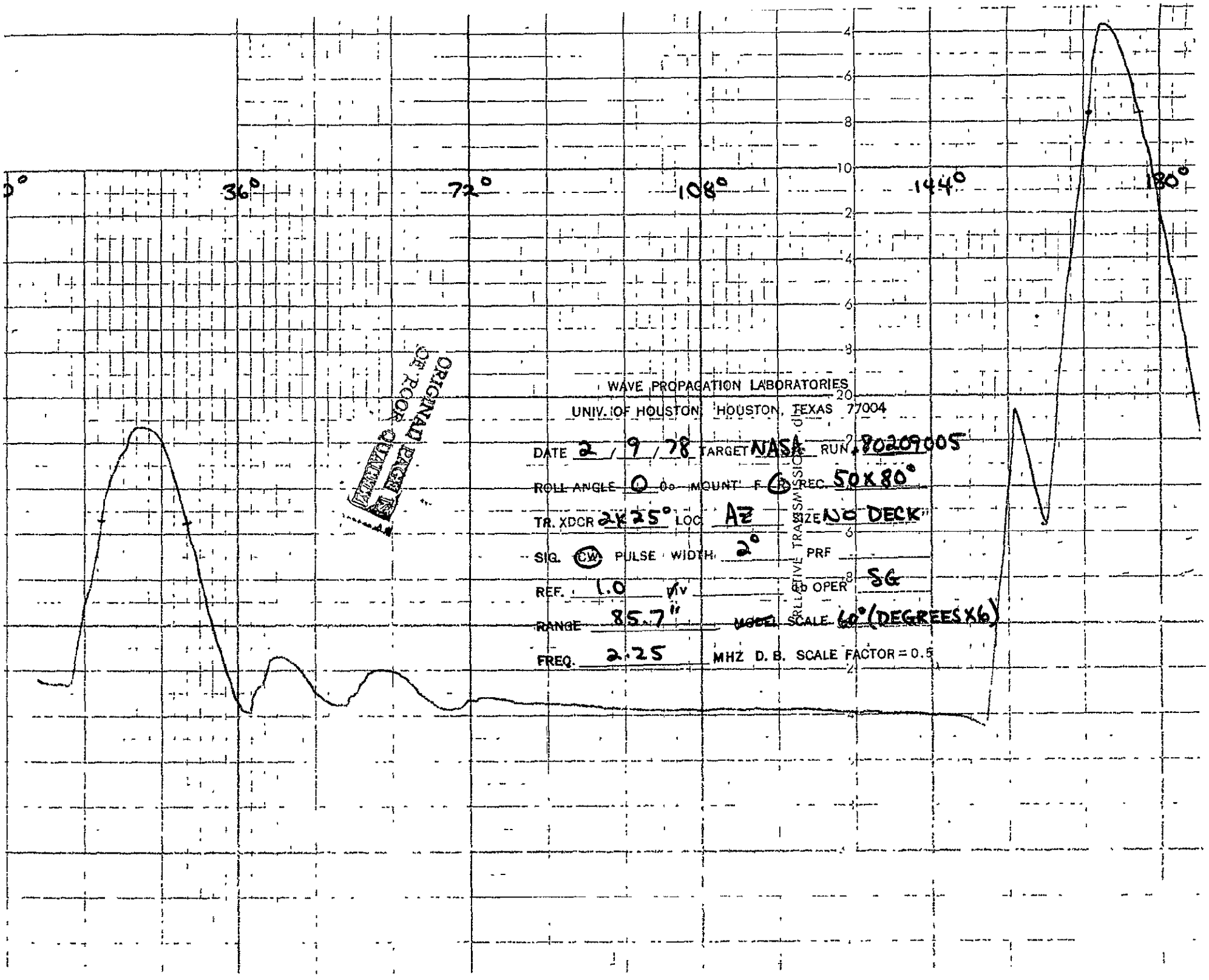
0°
36°
72°
108°
144°
180°
WAVE PROPAGATION LABORATORIES
UNIV. OF HOUSTON, HOUSTON, TEXAS 77004
DATE 2 / 9 / 78 TARGET NASA RUN 80209005
ROLL ANGLE 0 0o MOUNT F (B) REC 50X80°
TR. XDCR 2X25° LOC AZ SIZE 30" DECK
SIG. (CW) PULSE WIDTH 2° PRF
REF. 1.0 V/V OPER SG
RANGE 85.7" MODEL SCALE 60°(DEGREES X6)
FREQ. 2.25 MHZ D. B. SCALE FACTOR = 0.5
ORIGINAL PAGE IS OF POOR QUALITY

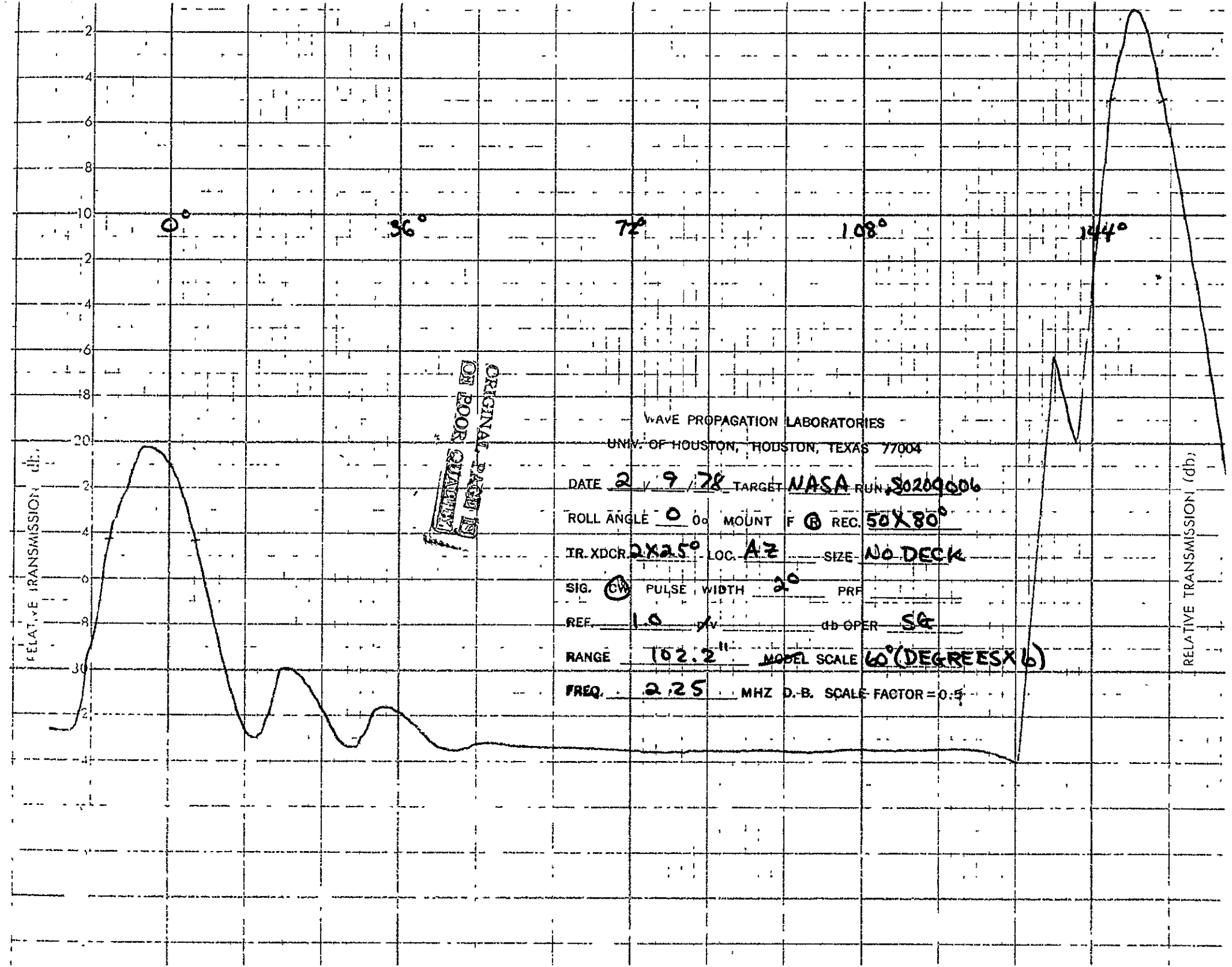
0°
36°
72°
108°
144°
RELATIVE TRANSMISSION (db)
RELATIVE TRANSMISSION (db)
ORIGINAL PAGE IS OF POOR QUALITY
WAVE PROPAGATION LABORATORIES
UNIV. OF HOUSTON, HOUSTON, TEXAS 77004
DATE 2/9/78 TARGET NASA RUN S0209006
ROLL ANGLE 0 0o MOUNT F @ REC. 50X80°
IR. XDCR 2X25° LOC. AZ SIZE NO DECK
SIG. CW PULSE WIDTH 20 PRF
REF. 1.0 V db OPER SG
RANGE 102.2" MODEL SCALE 60°(DEGREESX6)
FREQ. 2.25 MHZ D.-B. SCALE FACTOR = 0.5

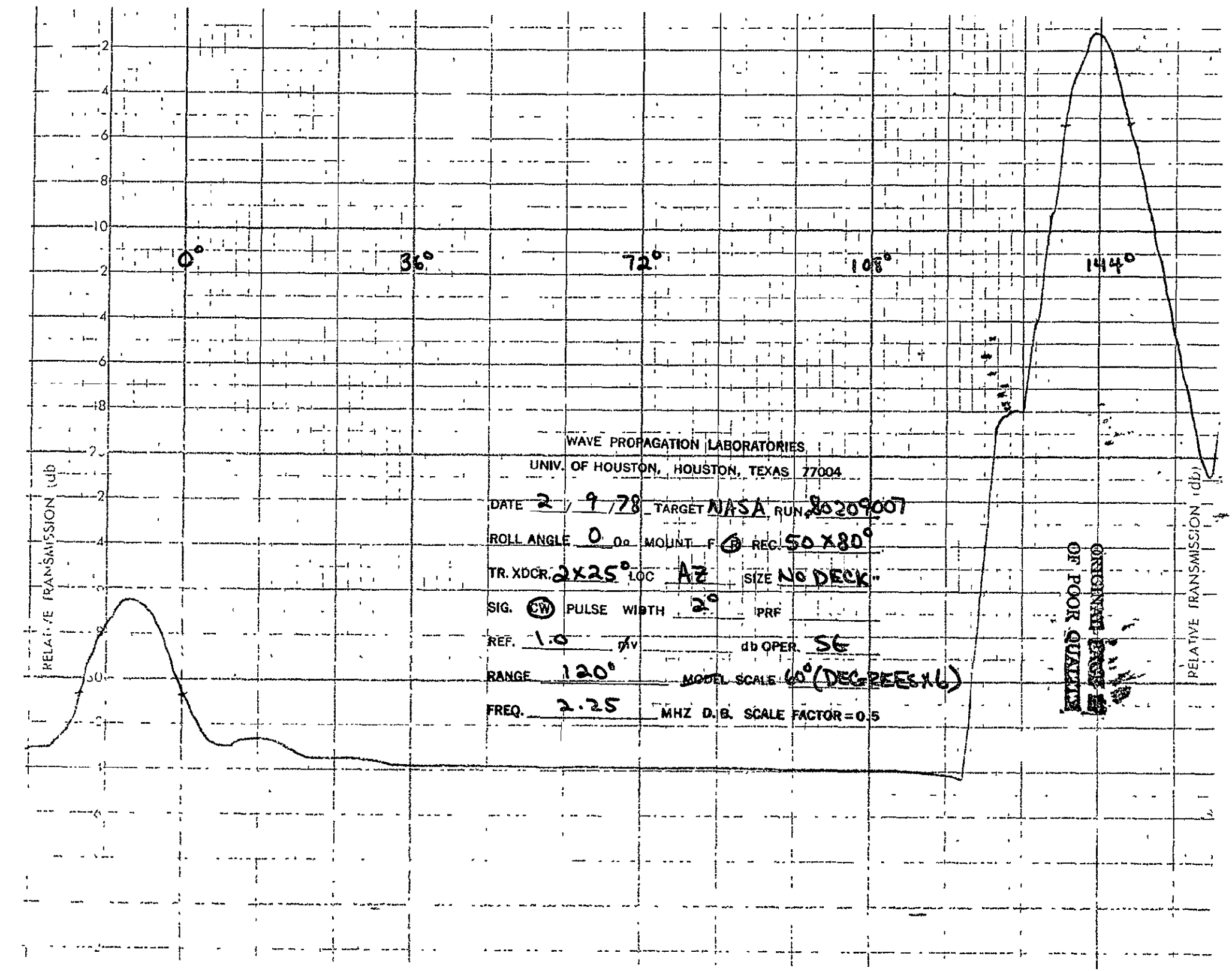
0°
36°
72°
108°
144°
RELATIVE TRANSMISSION (db)
RELATIVE TRANSMISSION (db)
WAVE PROPAGATION LABORATORIES
UNIV. OF HOUSTON, HOUSTON, TEXAS 77004
DATE 2 / 9 / 78 TARGET NASA RUN 80209007
ROLL ANGLE 0 00 MOUNT F/B REC. 50 x 80°
TR. XDCR. 2x25° LOC AZ SIZE NO DECK
SIG. CW PULSE WIDTH 20 PRF
REF. 1.0 nv db OPER. SE
RANGE 120° MODEL SCALE 60° (DEGREES x 2)
FREQ. 2.25 MHZ D.B. SCALE FACTOR = 0.5
ORIGINAL PAGE IS OF POOR QUALITY

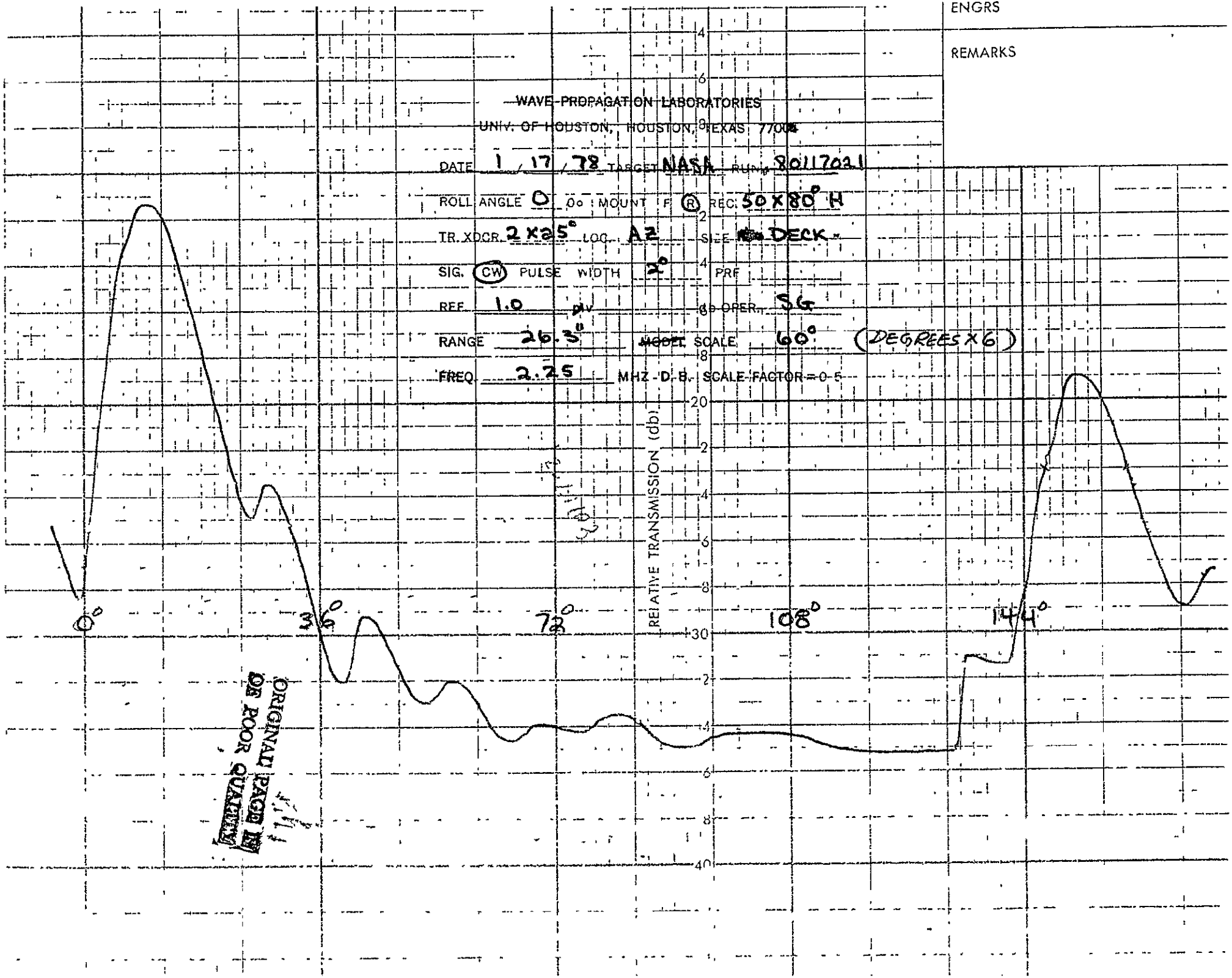
ENGRS
REMARKS
WAVE-PROPAGATION LABORATORIES
UNIV. OF HOUSTON, HOUSTON, TEXAS 77004
DATE 1 / 17 / 78 TARGET NASA RUN 8011702.1
ROLL ANGLE 0 .0o MOUNT F (R) REC. 50 X 80° H
TR. XDCR 2 X 25° LOC. A2 SIZE DECK
SIG. (CW) PULSE WIDTH PRF
REF 1.0 dV dB ORDER SG
RANGE 26.3" MODEL SCALE 60° (DEGREES X 6)
FREQ. 2.25 MHZ - D.B. SCALE FACTOR = 0-5
RELATIVE TRANSMISSION (db)
0
2
4
6
8
10
20
30
40
0°
36°
72°
108°
144°
ORIGINAL PAGE IS OF POOR QUALITY

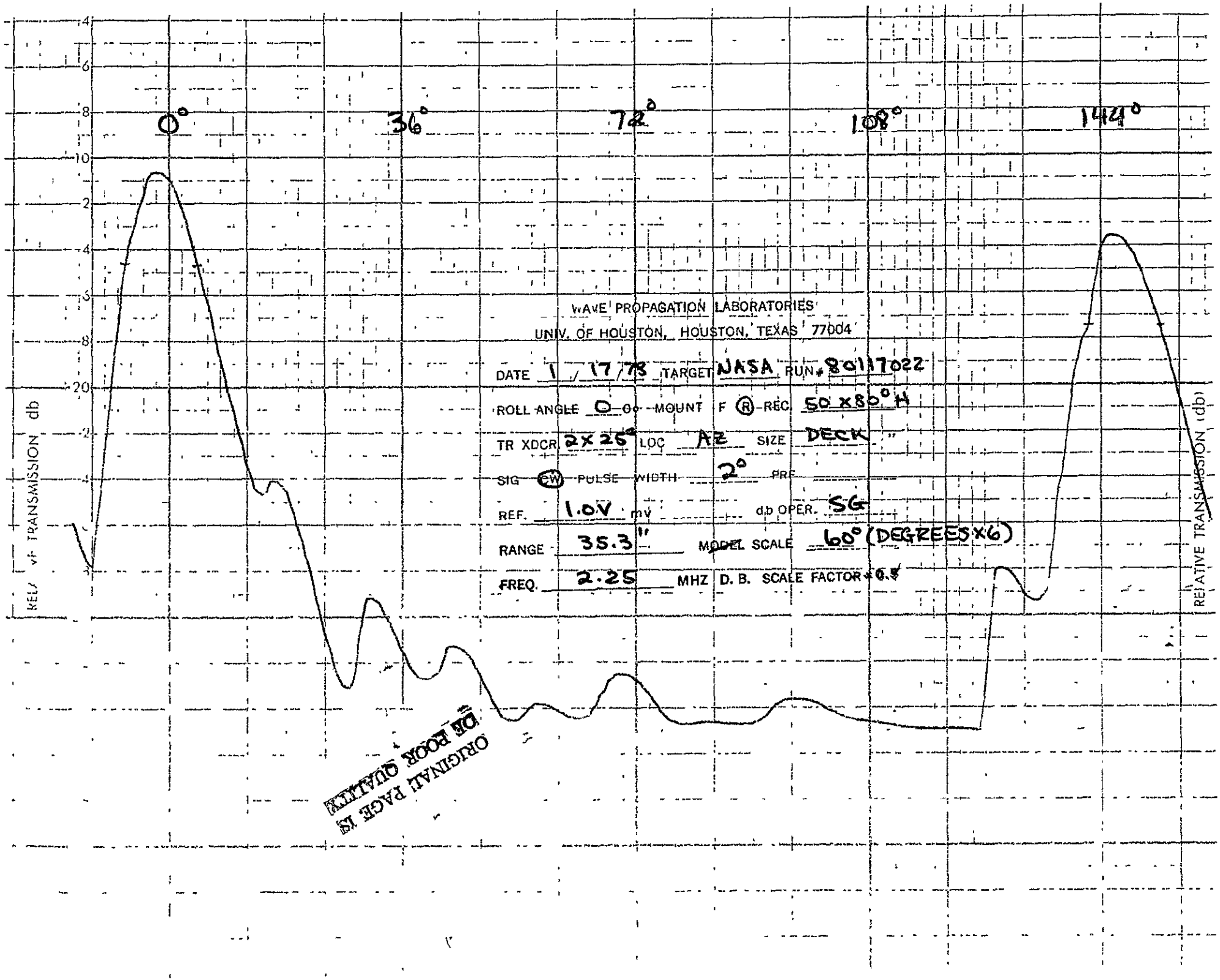
0°
36°
72°
108°
144°
WAVE PROPAGATION LABORATORIES
UNIV. OF HOUSTON, HOUSTON, TEXAS 77004
DATE 1/17/73 TARGET NASA RUN# 80117022
ROLL ANGLE 0 0c MOUNT F (R) REC 50 x 80° H
TR XDCR 2x25° LOC AZ SIZE DECK "
SIG (CW) PULSE WIDTH 2° PRF
REF. 1.0V mv db OPER. SG
RANGE 35.3" MODEL SCALE 60° (DEGREES x6)
FREQ. 2.25 MHZ D. B. SCALE FACTOR = 0.5
REL. TRANSMISSION db
RELATIVE TRANSMISSION (db)
ORIGINAL PAGE IS OF POOR QUALITY

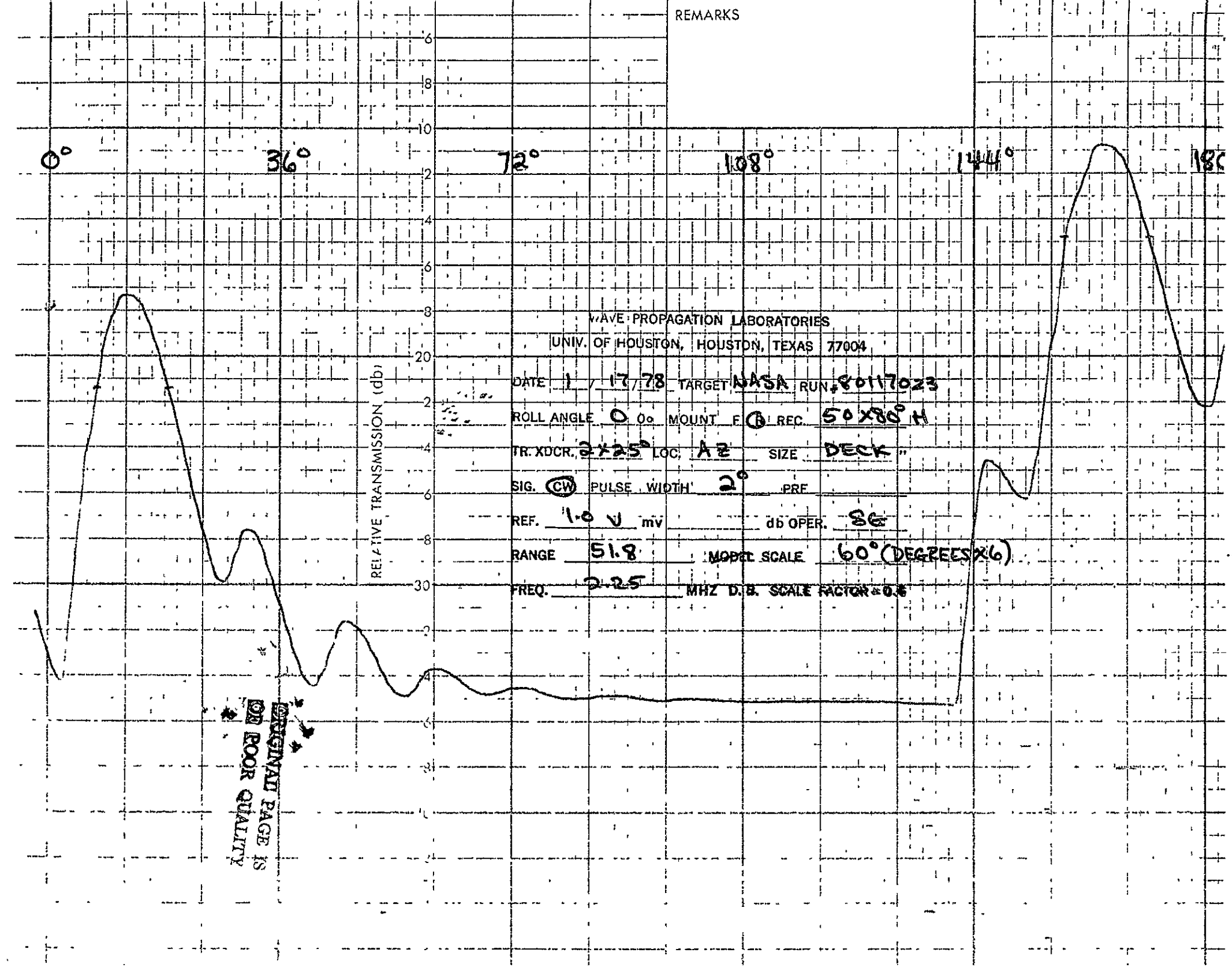
REMARKS
0°
36°
72°
108°
144°
180
RELATIVE TRANSMISSION (db)
WAVE PROPAGATION LABORATORIES
UNIV. OF HOUSTON, HOUSTON, TEXAS 77004
DATE 1 / 17 / 78 TARGET NASA RUN # 80117023
ROLL ANGLE 0 0o MOUNT F B REC 50 X 80° H
TR. XDCR. 2 X 25° LOC. A2 SIZE DECK "
SIG. CW PULSE WIDTH 2° PRF
REF. 1.0 V mv db OPER. SG
RANGE 51.8 MODEL SCALE 60° (DEGREES X6)
FREQ. 2.25 MHZ D.B. SCALE FACTOR = 0.6
ORIGINAL PAGE IS
OF POOR QUALITY

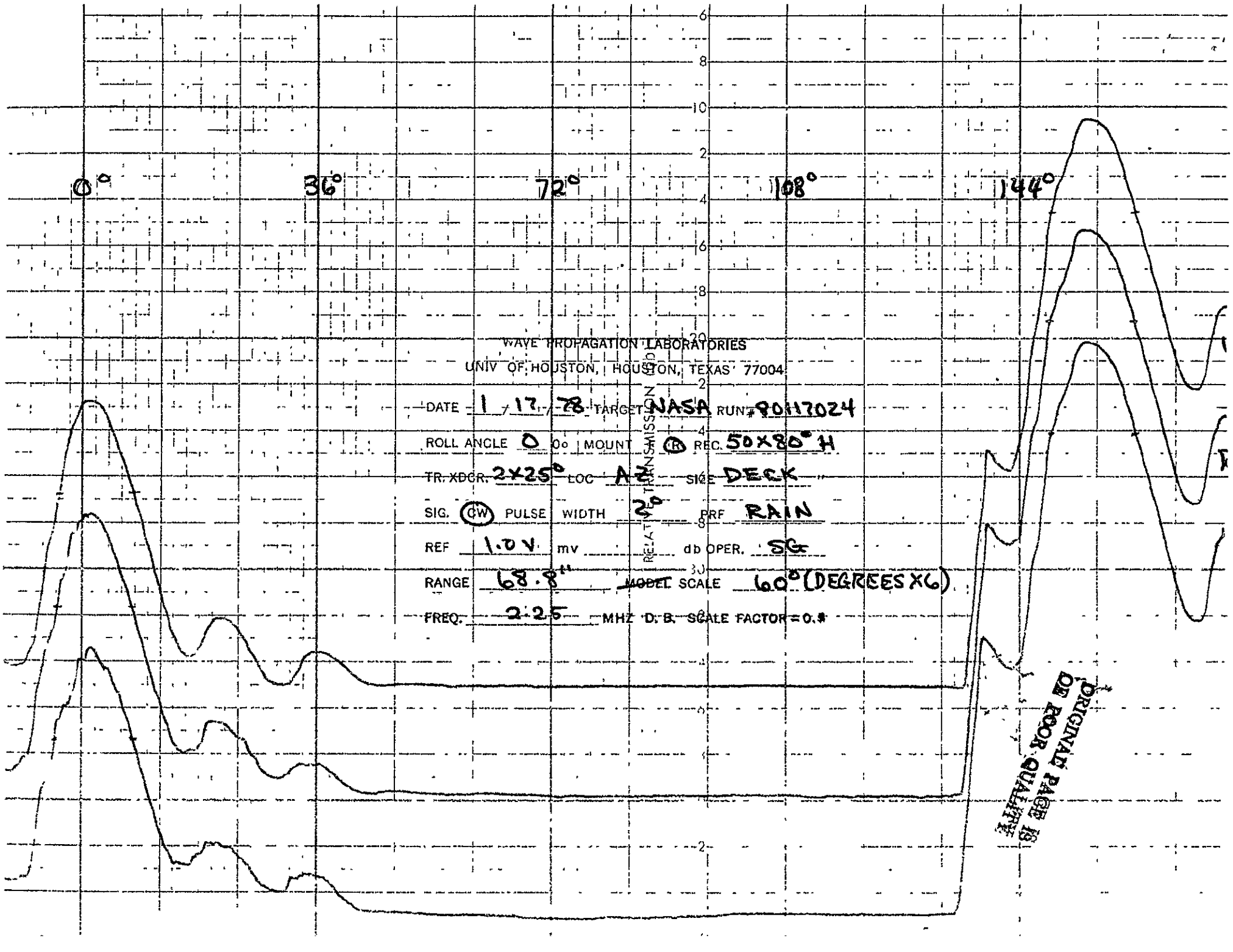
0°
36°
72°
108°
144°
WAVE PROPAGATION LABORATORIES
UNIV OF HOUSTON, HOUSTON, TEXAS 77004
DATE 1/17/78 TARGET NASA RUN# 80117024
ROLL ANGLE 0 0o MOUNT CR REC. 50x80° H
TR. XDCR. 2x25° LOC A-4 SIZE DECK
SIG. CW PULSE WIDTH 2μ PRF RAIN
REF 1.0 V mv db OPER. SG
RANGE 68.8" MODEL SCALE 60° (DEGREES X6)
FREQ. 2.25 MHZ D. B. SCALE FACTOR = 0.*
RELATIVE TRANSMISSION
ORIGINAL PAGE IS OF POOR QUALITY

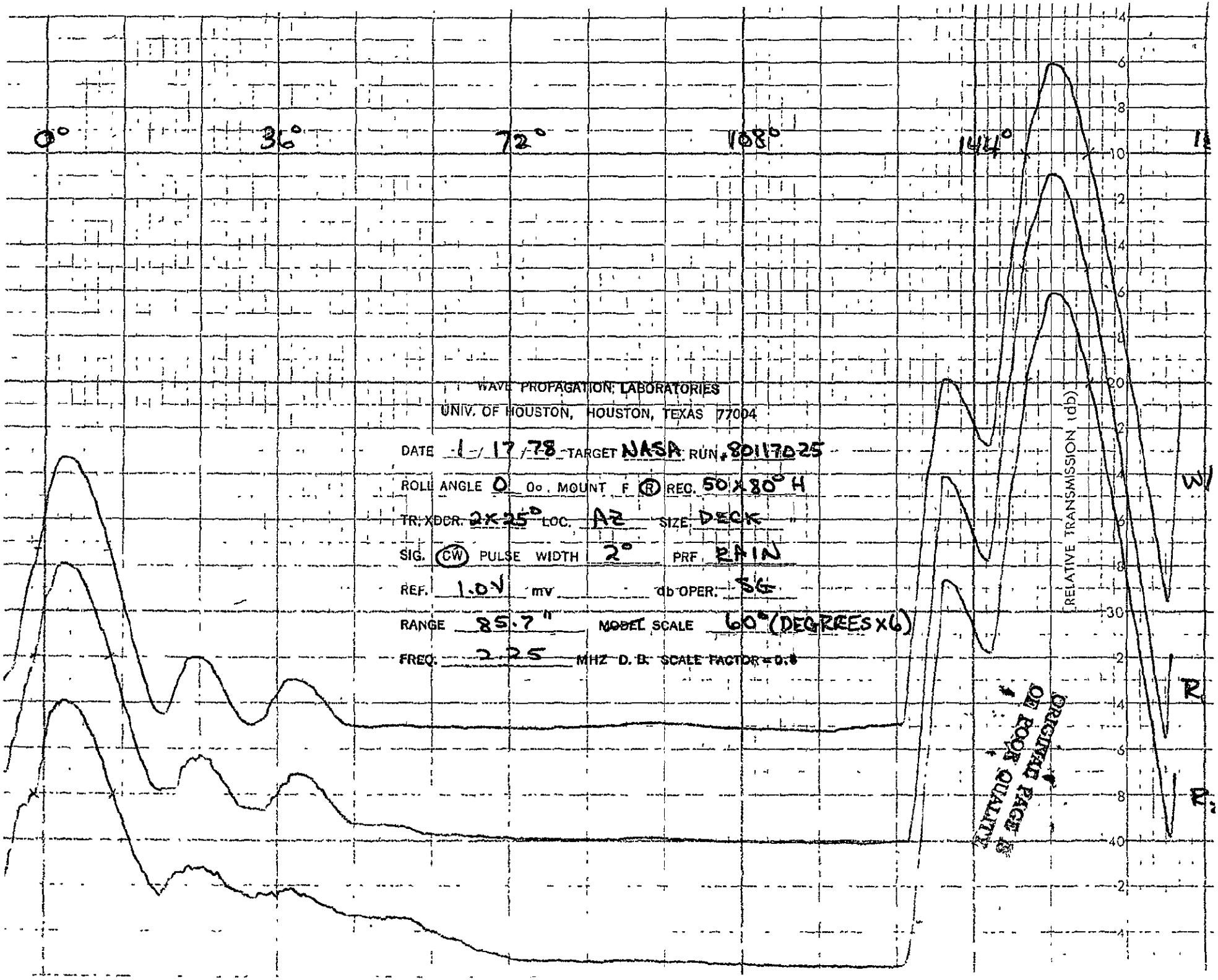
0°
36°
72°
108°
144°
WAVE PROPAGATION LABORATORIES
UNIV. OF HOUSTON, HOUSTON, TEXAS 77004
DATE 1-17-78 TARGET NASA RUN 80117025
ROLL ANGLE 0 0o. MOUNT F (R) REC. 50x80° H
TR. XDCR. 2x25° LOC. A2 SIZE DECK
SIG. (CW) PULSE WIDTH 2° PRF RAIN
REF. 1.0V mv db OPER. SG
RANGE 85.7" MODEL SCALE 60°(DEGREES x 6)
FREQ. 2.25 MHZ D. B. SCALE FACTOR = 0.8
RELATIVE TRANSMISSION (dB)
W
R
R'
ORIGINAL PAGE IS OF POOR QUALITY

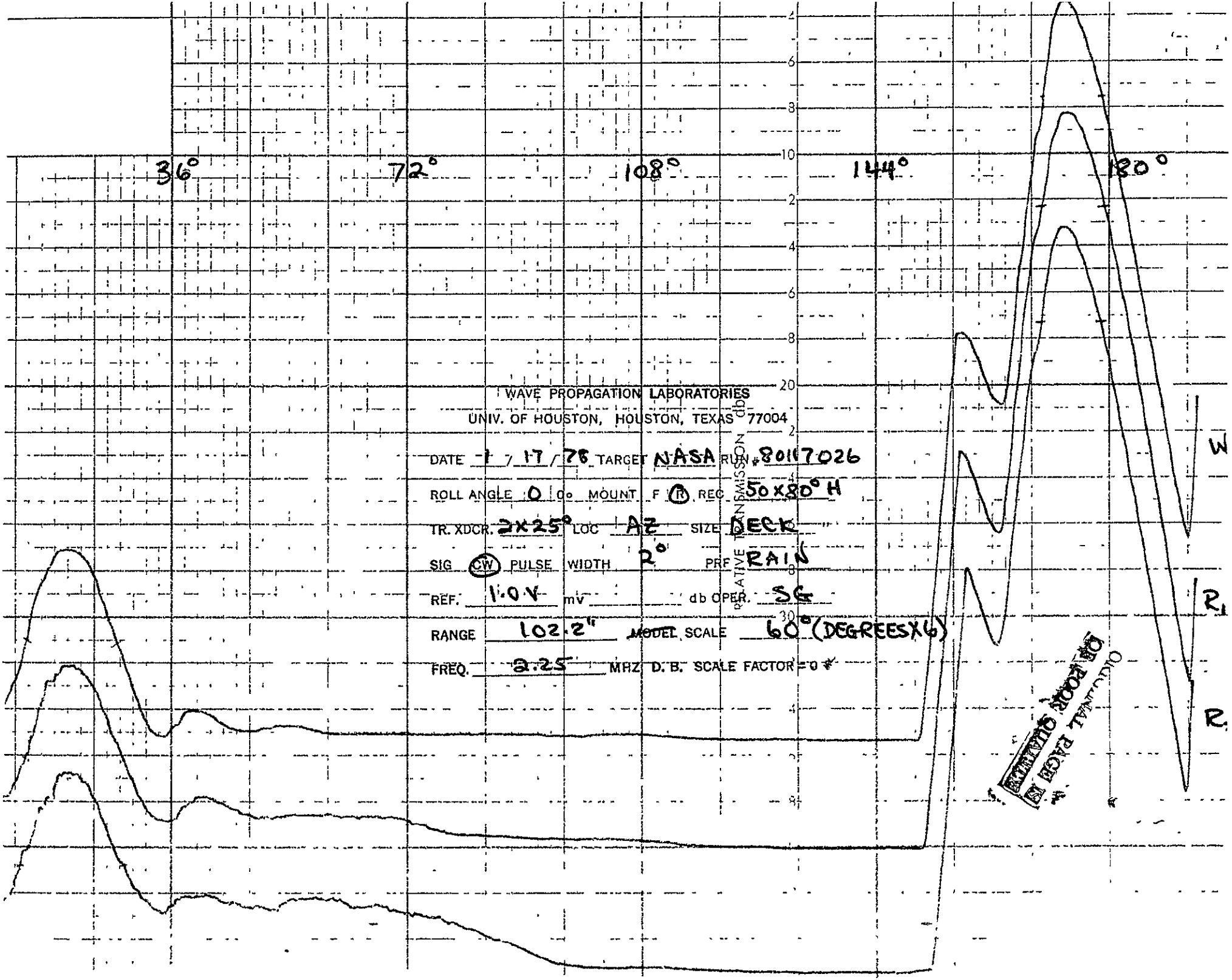
36°
72°
108°
144°
180°
WAVE PROPAGATION LABORATORIES
UNIV. OF HOUSTON, HOUSTON, TEXAS 77004
DATE 1 / 17 / 76 TARGET NASA RUN # 80117026
ROLL ANGLE 0 0° MOUNT F (R) REC 50x80° H
TR. XDCR. 2x25° LOC AZ SIZE DECK
SIG (CW) PULSE WIDTH 2° PRF RAIN
REF. 1.0 V mv db OPER. SG
RANGE 102.2" MODEL SCALE 60° (DEGREES X 6)
FREQ. 2.25 MHZ D. B. SCALE FACTOR = 0
RELATIVE TRANSMISSION db
W
R1
R2
ORIGINAL PAGE IS OF POOR QUALITY

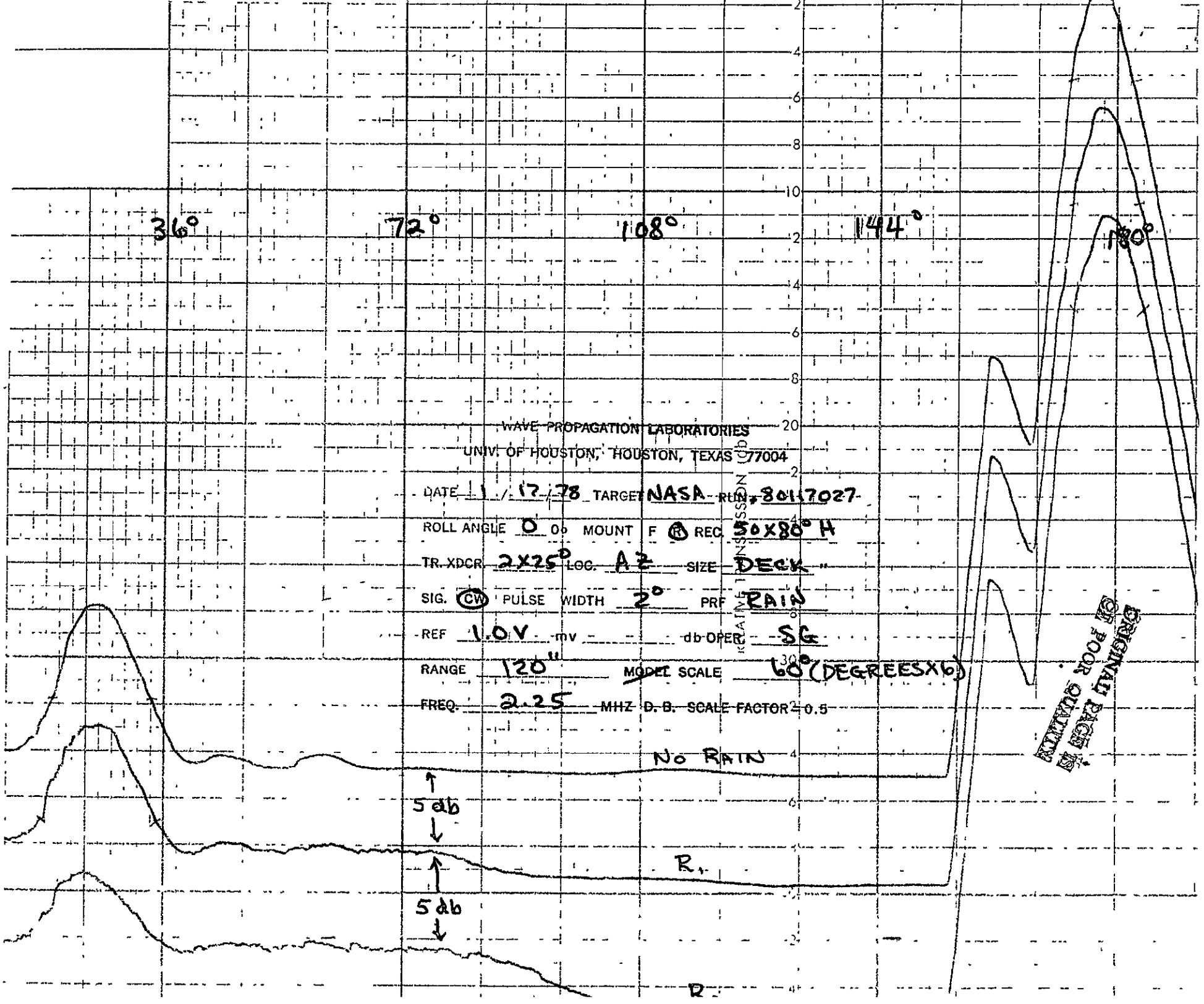
360°
72°
108°
144°
180°
WAVE PROPAGATION LABORATORIES
UNIV. OF HOUSTON, HOUSTON, TEXAS 77004
DATE 1/17/78 TARGET NASA RUN 80117027
ROLL ANGLE 0 0b MOUNT F R REC 50X80° H
TR. XDCR 2X25° LOC. A2 SIZE DECK "
SIG. CW PULSE WIDTH 2° PRF RAIN
REF 1.0V mv db OPER SG
RANGE 120" MODEL SCALE 60°(DEGREESX6)
FREQ. 2.25 MHZ D. B. SCALE FACTOR 0.5
RELATIVE TRANSMISSION (db)
No RAIN
5 db
5 db
R
R
ORIGINAL PAGE IS
OF POOR QUALITY

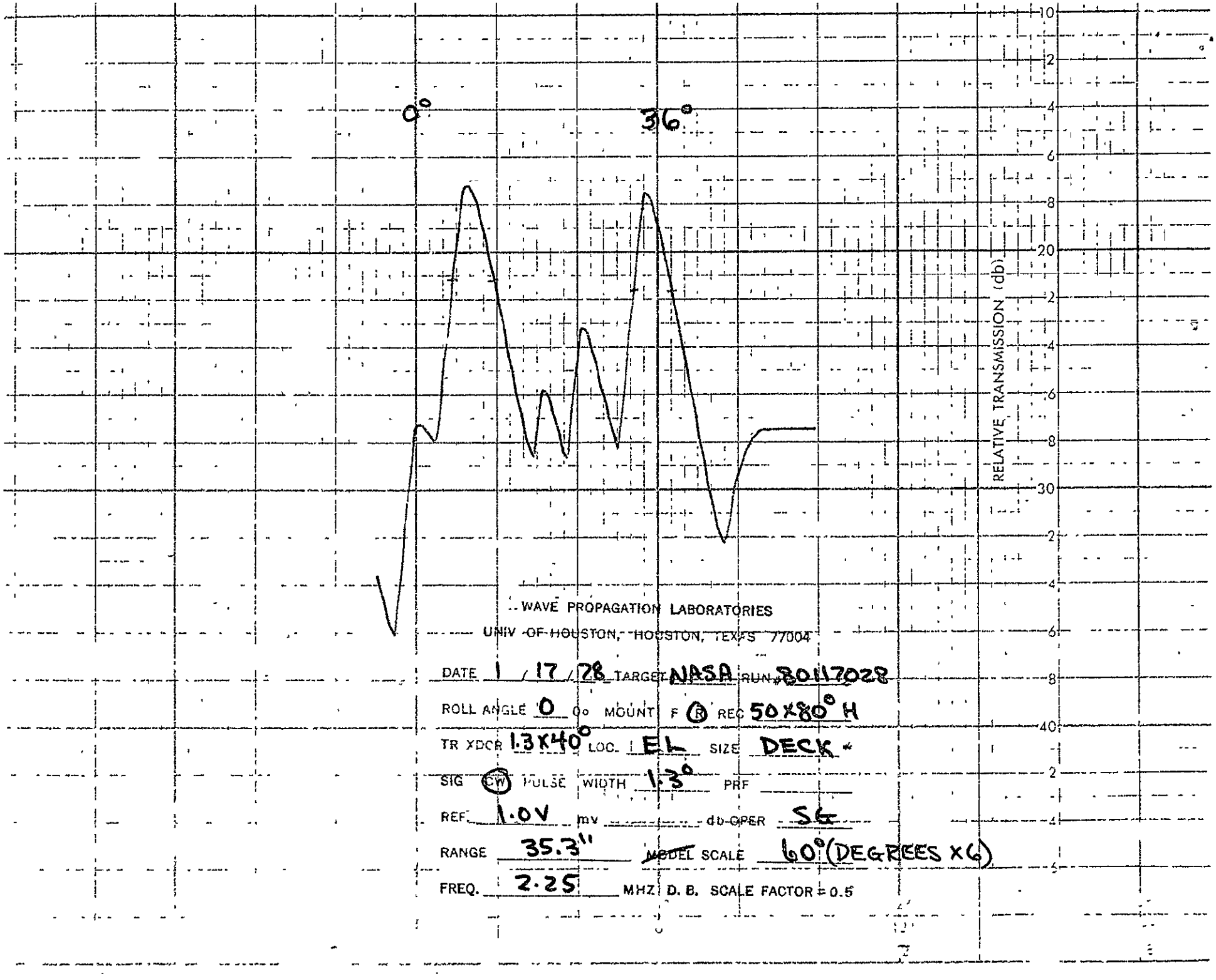
0°
36°
RELATIVE TRANSMISSION (db)
10
2
4
6
8
20
2
4
6
8
30
2
4
6
8
40
2
4
WAVE PROPAGATION LABORATORIES
UNIV OF HOUSTON, HOUSTON, TEXAS 77004
DATE 1 / 17 / 78 TARGET NASA RUN # 80117028
ROLL ANGLE 0 0o MOUNT F (R) REC 50x80° H
TR XDCR 1.3x40° LOC. EL SIZE DECK "
SIG (CW) PULSE WIDTH 1.3° PRF
REF 1.0V mv db-OPER S6
RANGE 35.3" MODEL SCALE 60° (DEGREES x6)
FREQ. 2.25 MHZ D. B. SCALE FACTOR = 0.5

OJECT

IGRS

MARKS

WAVE PROPAGATION LABORATORIES

UNIV OF HOUSTON, HOUSTON, TEXAS 77004

DATE 1 / 17 / 78 TARGET NASA RUN # 80117029

ROLL ANGLE 0 00 MOUNT F (R) REC. 50×80° H

TR XDCR. 1.3 H 40° LOC EH SIZE DECK "

SIG (CW) PULSE WIDTH 1.3° PRF "

REF 1.0 V mV db OPER SG

RANGE 51.8" MODEL SCALE 60° (DEGREES X 6)

FREQ. 3.25 MHZ D.B. SCALE FACTOR = 0 5

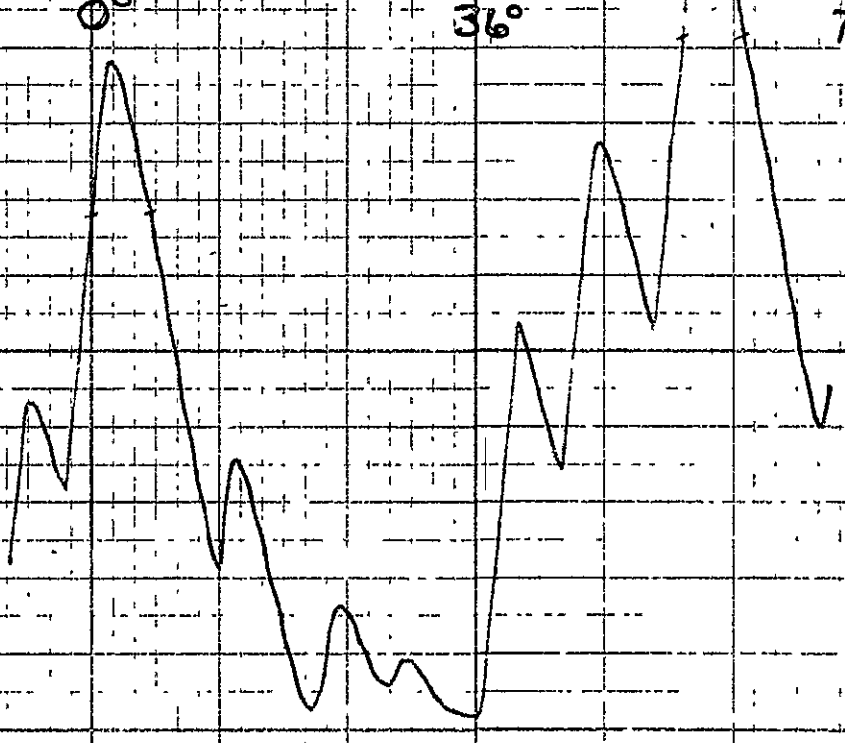

RELATIVE TRANSMISSION db

6 3 10 0 8 20 2 4 6 8 30 2 4 6 8 40 2

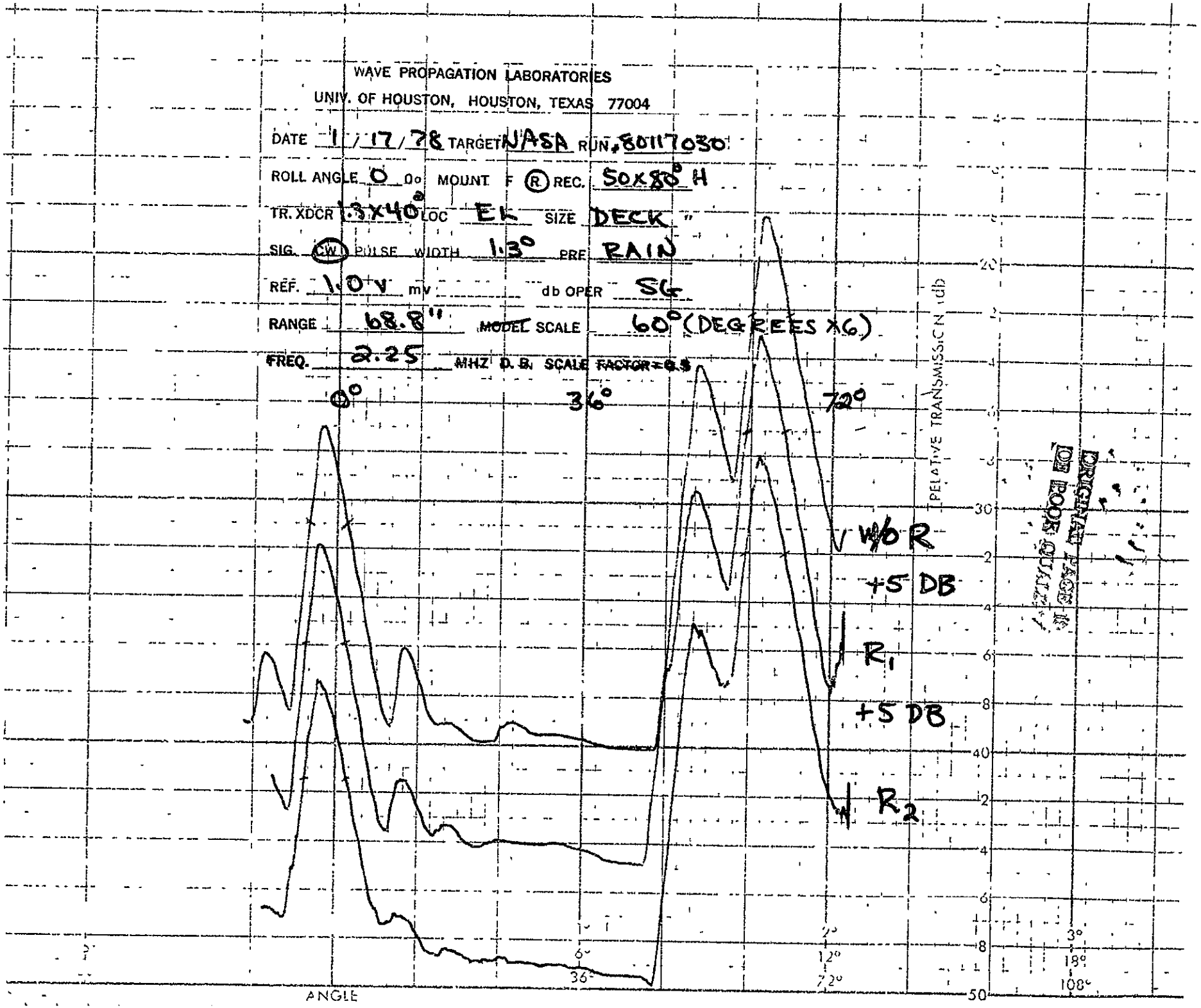
WAVE PROPAGATION LABORATORIES
UNIV. OF HOUSTON, HOUSTON, TEXAS 77004
DATE 1/17/78 TARGET NASA RUN 80117030
ROLL ANGLE 0 0° MOUNT F (R) REC. 50x80° H
TR. XDCR 1.3x40° LOC EL SIZE DECK "
SIG. (CW) PULSE WIDTH 1.3° PRF RAIN
REF. 1.0 V mV db OPER SG
RANGE 68.8" MODEL SCALE 60° (DEGREES x6)
FREQ. 2.25 MHZ D. B. SCALE FACTOR = 0.5
0°
36°
72°
W/O R
+5 DB
R1
+5 DB
R2
RELATIVE TRANSMISSION (db)
ORIGINAL PAGE IS OF POOR QUALITY
ANGLE
6°
36°
12°
72°
18°
108°

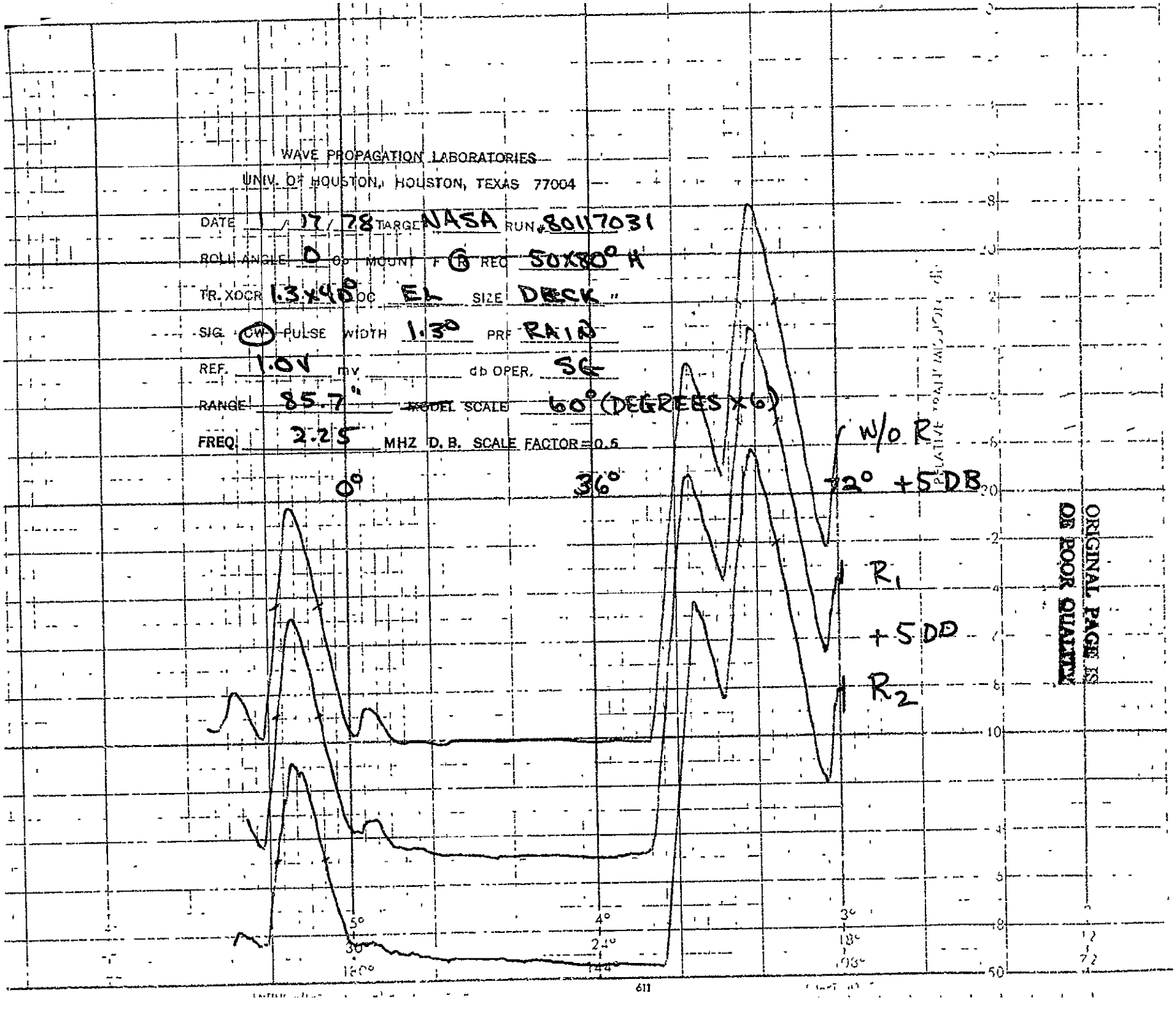
WAVE PROPAGATION LABORATORIES
UNIV. OF HOUSTON, HOUSTON, TEXAS 77004
DATE 12/78 TARGET NASA RUN 80117031
ROLL ANGLE 0 deg MOUNT F (B) REC 50X80° H
TR. XDCR 1.3x40° DC EL SIZE DECK"
SIG (CW) PULSE WIDTH 1.3° PRF RAID
REF. 1.0V mv db OPER. SC
RANGE 85.7" MODEL SCALE 60° (DEGREES x 6)
FREQ. 2.25 MHZ D.B. SCALE FACTOR = 0.5
0°
36°
72°
+5 DB
W/O R
R1
+5 DD
R2
ORIGINAL PAGE IS OF POOR QUALITY
RELATIVE POWER (DB)
611

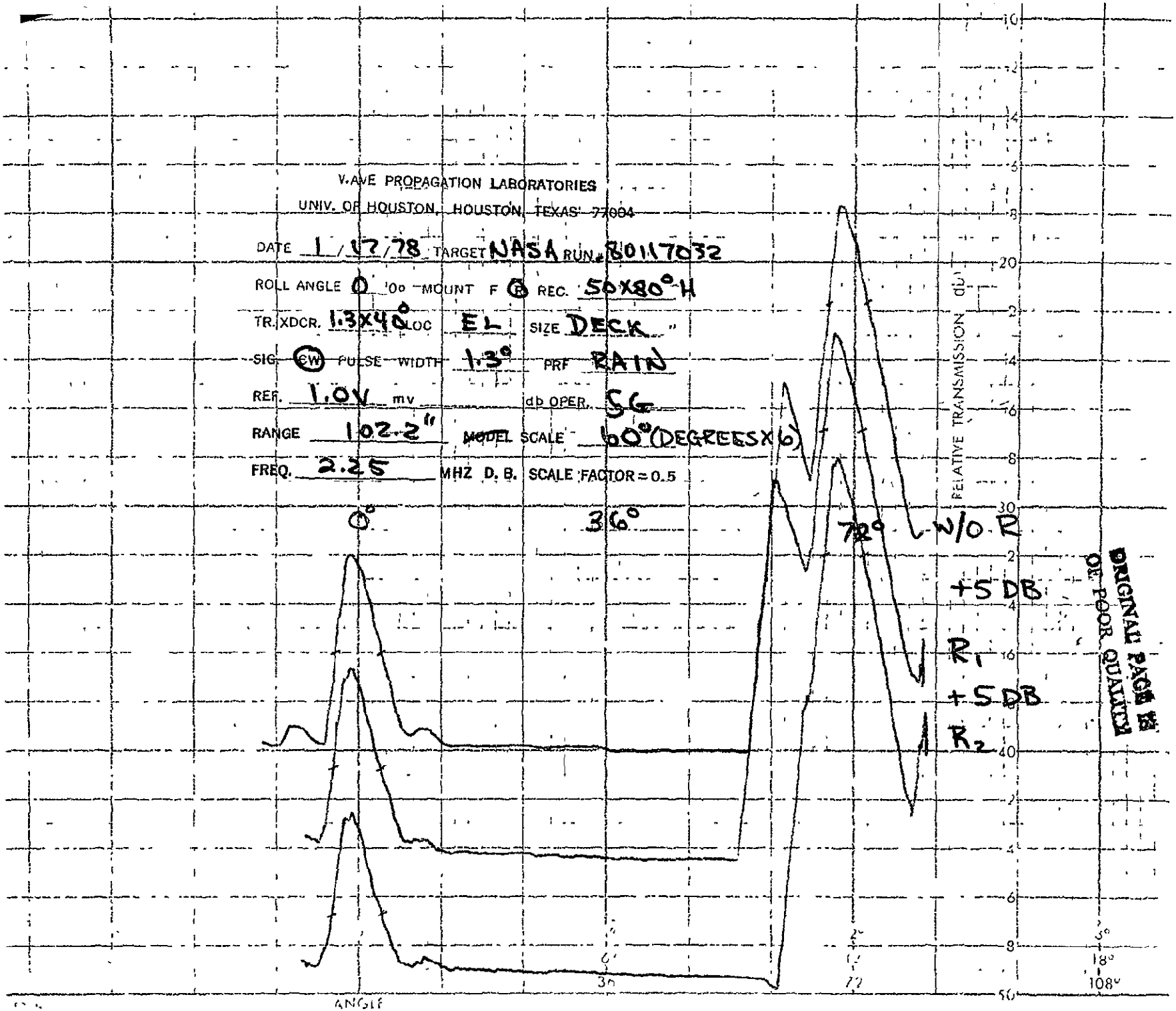
WAVE PROPAGATION LABORATORIES
UNIV. OF HOUSTON, HOUSTON, TEXAS 77004
DATE 1/17/78 TARGET NASA RUN# 80117032
ROLL ANGLE 0 00 MOUNT F (B) REC. 50x80°H
TR. XDCR. 1.3x40° LOC EL SIZE DECK "
SIG (CW) PULSE WIDTH 1.3° PRF RAIN
REF. 1.0V mv dB OPER. SG
RANGE 102.2" MODEL SCALE 60°(DEGREESX6)
FREQ. 2.25 MHZ D. B. SCALE FACTOR = 0.5
0°
36°
72°
w/o R
+5 DB
R1
+5 DB
R2
RELATIVE TRANSMISSION dB
ANGLE
ORIGINAL PAGE IS OF POOR QUALITY

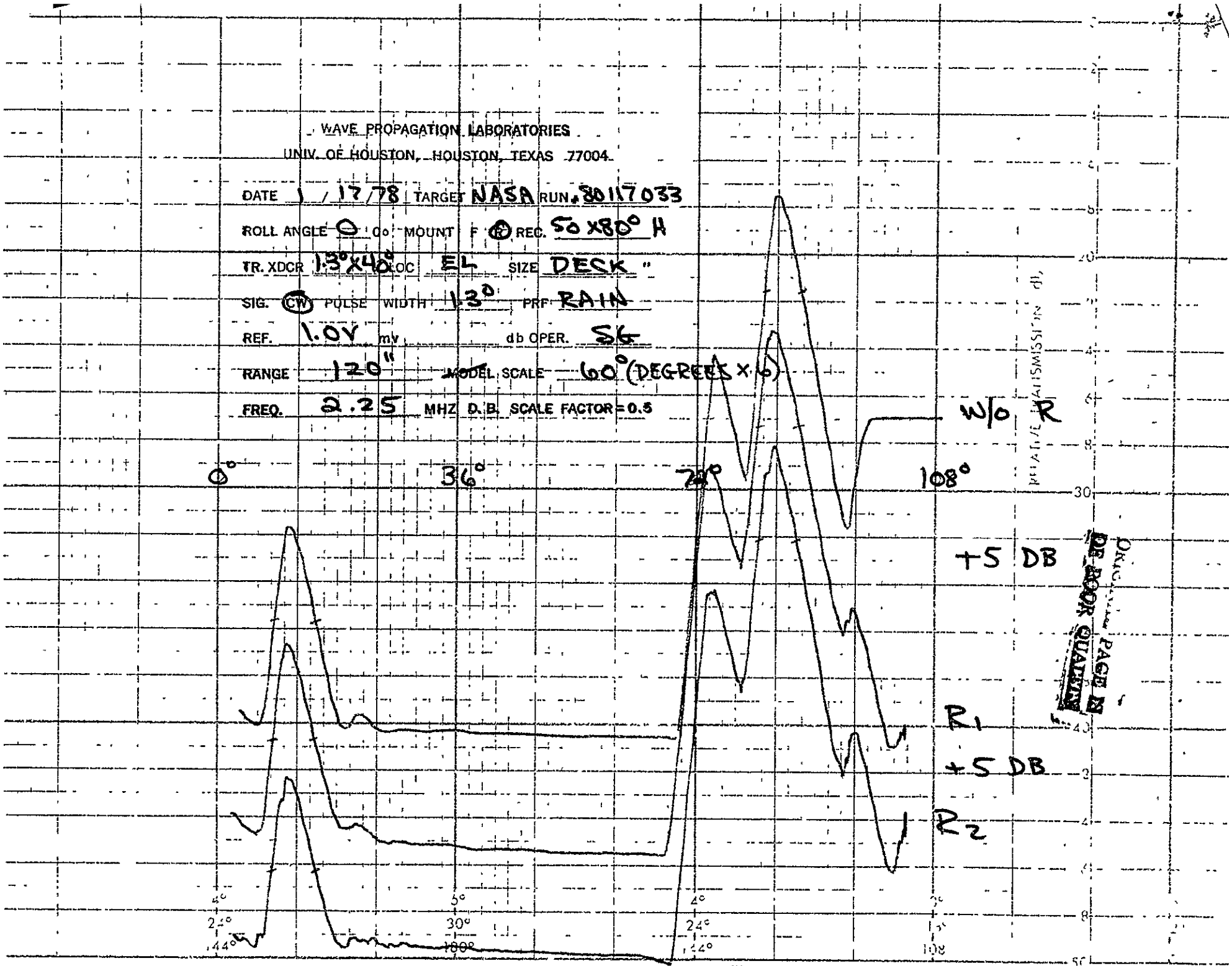
WAVE PROPAGATION LABORATORIES
UNIV. OF HOUSTON, HOUSTON, TEXAS 77004
DATE 1 / 17 / 78 TARGET NASA RUN # 80117033
ROLL ANGLE 0 00 MOUNT F R REC. 50 x 80° H
TR. XDCR 1.3°X4° LOC EL SIZE DESK "
SIG. CW POLSE WIDTH 13° PRF RAIN
REF. 1.0V mv db OPER. 56
RANGE 120" MODEL SCALE 60° (DEGREES x 6)
FREQ. 2.25 MHZ D.B. SCALE FACTOR = 0.5
0°
36°
24°
108°
W/O R
+5 DB
R1
+5 DB
R2
4°
5°
4°
30°
24°
44°
180°
44°
108
30
8
4
3
8
50
PATTERN TRANSMISSION dB
PAGE IS POOR QUALITY
611